

1 **Neutralizing and protective human monoclonal antibodies recognizing the N-**
2 **terminal domain of the SARS-CoV-2 spike protein**

3
4 Naveenchandra Suryadevara^{1,#}, Swathi Shrihari^{4#}, Pavlo Gilchuk¹, Laura A. VanBlargan⁴, Elad
5 Binshtein¹, Seth J. Zost¹, Rachel S. Nargi¹, Rachel E. Sutton¹, Emma S. Winkler^{3,4}, Elaine C.
6 Chen⁵, Mallorie E. Fouch⁶, Edgar Davidson⁶, Benjamin J. Doranz⁶, Robert H. Carnahan^{1,7}, Larissa
7 B. Thackray^{4,*}, Michael S. Diamond^{2,3,4,8,*}, and James E. Crowe, Jr.^{1,5,7,*}

8
9 ¹Vanderbilt Vaccine Center, Vanderbilt University Medical Center, Nashville, TN, 37232, USA

10 ²Department of Molecular Microbiology, Washington University School of Medicine, Saint
11 Louis, MO, 63110, USA

12 ³Department of Pathology and Immunology, Washington University School of Medicine, Saint
13 Louis, MO, 63110, USA

14 ⁴Department of Medicine, Washington University School of Medicine, Saint Louis, MO, 63110
15 USA

16 ⁵Department of Pathology, Microbiology and Immunology, Vanderbilt University Medical
17 Center, Nashville, TN, 37232, USA

18 ⁶Integral Molecular, Philadelphia, PA, 19104, USA

19 ⁷Department of Pediatrics, Vanderbilt University Medical Center, Nashville, TN, 37232, USA

20 ⁸Andrew M. and Jane M. Bursky Center for Human Immunology and Immunotherapy
21 Programs, Washington University School of Medicine, Saint Louis, MO, 63110, USA

22 # These authors contributed equally.

23 *Corresponding authors. Lead Contact: james.crowe@vumc.org

24

25 **SUMMARY**

26 Most human monoclonal antibodies (mAbs) neutralizing SARS-CoV-2 recognize the spike
27 (S) protein receptor-binding domain and block virus interactions with the cellular receptor
28 angiotensin-converting enzyme 2. We describe a panel of human mAbs binding to diverse epitopes
29 on the N-terminal domain (NTD) of S protein from SARS-CoV-2 convalescent donors and found
30 a minority of these possessed neutralizing activity. Two mAbs (COV2-2676 and COV2-2489)
31 inhibited infection of authentic SARS-CoV-2 and recombinant VSV/SARS-CoV-2 viruses. We
32 mapped their binding epitopes by alanine-scanning mutagenesis and selection of functional SARS-
33 CoV-2 S neutralization escape variants. Mechanistic studies showed that these antibodies
34 neutralize in part by inhibiting a post-attachment step in the infection cycle. COV2-2676 and
35 COV2-2489 offered protection either as prophylaxis or therapy, and Fc effector functions were
36 required for optimal protection. Thus, natural infection induces a subset of potent NTD-specific
37 mAbs that leverage neutralizing and Fc-mediated activities to protect against SARS-CoV-2
38 infection using multiple functional attributes.

39

40 **Keywords:** Coronavirus; SARS-CoV-2; Antibodies, Monoclonal; Antibodies, Neutralizing;
41 Antibodies, Viral; SARS-CoV-2; N-terminal domain

42 INTRODUCTION

43 Since the emergence of severe acute respiratory syndrome coronavirus 2 (SARS-CoV-2)
44 as a major threat to global public health, many studies have focused efforts on discovery of potent
45 neutralizing monoclonal antibodies (mAbs) against the spike (S) protein of SARS-CoV-2 (Baum
46 et al., 2020a; Cao et al., 2020; Hansen et al., 2020; Ju et al., 2020; Liu et al., 2020a; Pinto et al.,
47 2020; Robbiani et al., 2020; Zost et al., 2020b). The S protein exists as a trimer on the surface of
48 SARS-CoV-2 and facilitates entry of the virus into cells. The receptor binding domain (RBD)
49 situated in the S1 region of the S protein binds to human angiotensin-converting enzyme 2
50 (hACE2). The S2 region then changes conformation and inserts its fusion peptide into the target
51 cell membrane, thus triggering viral fusion and entry. Previous studies have demonstrated that the
52 RBD region is a key target for potently neutralizing antibodies (Alsoussi et al., 2020; Barnes et al.,
53 2020; Baum et al., 2020a; Hansen et al., 2020; Hassan et al., 2020; Zost et al., 2020a). These
54 studies also defined inhibition of S trimer binding to the cellular receptor ACE2 as a principal
55 mechanism of action of RBD-targeting antibodies against SARS-CoV-2, and showed protection
56 in animals against infection and disease by this class of mAbs (Baum et al., 2020a; Hansen et al.,
57 2020; Hassan et al., 2020; Zost et al., 2020a).

58 Since the start of the outbreak, circulating SARS-CoV-2 field strains have acquired genetic
59 changes that facilitate transmission (Avanzato et al., 2020; Choi et al., 2020; Hou et al., 2020;
60 Kemp et al., 2020; McCarthy et al., 2020; Plante et al., 2020; Rambaut et al., 2020; Tegally et al.,
61 2020). This rapid viral evolution also could affect the protective efficacy of vaccines and mAb-
62 based therapeutics currently in clinical trials or approved under emergency use authorization. Most
63 of the mAbs under evaluation in clinical trials or authorized for the emergency use bind to the
64 RBD (Baum et al., 2020a; Zost et al., 2020a). Several groups have described mAbs targeting non-

65 RBD regions, but their epitopes, mechanisms of action, and protective activity *in vivo* remain
66 unclear (Chi et al., 2020; Liu et al., 2020a). Here we define the structure-function relationship of
67 potent NTD-reactive antibodies from a panel of 389 human SARS-CoV-2 S protein mAbs we
68 isolated from survivors of natural infection (Zost et al., 2020a; Zost et al., 2020b). We found 43
69 mAbs recognizing the NTD. Three of the 43 NTD-reactive mAbs exhibited neutralizing capacity
70 against authentic SARS-CoV-2 virus (Zost et al., 2020b), with two being potently inhibitory. We
71 mapped the epitopes for the two most potently neutralizing NTD-reactive mAbs and dissected the
72 mechanism by which these mAbs inhibited SARS-CoV-2 infection. These two mAbs conferred
73 protection in hACE2-expressing mice when administered either as prophylaxis or therapy, and
74 intact Fc effector functions were required for optimal activity *in vivo*. Thus, we show that regions
75 of the NTD are recognized by neutralizing and protective antibodies against SARS-CoV-2 and
76 could function as part of antibody cocktails to minimize the selection of escape variants or
77 resistance to natural variants in RBD as they emerge.

78

79 RESULTS

80 Two non-RBD anti-SARS-CoV-2 S-protein-specific mAbs potently neutralize virus.

81 We previously isolated 389 SARS-CoV-2 reactive mAbs from the B cells of convalescent COVID-
82 19 patients. While most of the neutralizing antibodies mapped to the RBD and blocked ACE2
83 binding to the S protein, multiple neutralizing mAbs that did not bind RBD were also identified
84 (Zost et al., 2020a; Zost et al., 2020b). We selected the two most potently neutralizing S-protein-
85 reactive mAbs that did not bind to RBD, designated COV2-2676 and COV2-2489, for further
86 study. We first assessed binding and neutralizing activities of COV2-2676 and COV2-2489 to
87 determine their potency. Both mAbs bound weakly to a recombinant SARS-CoV-2 S6P_{ecto} protein
88 expressed as a trimer, but failed to react with a recombinant soluble NTD protein. In contrast,
89 additional SARS-CoV-2-specific non-RBD mAbs, COV2-2263 and COV2-2490, which are non-
90 neutralizing(Zost et al., 2020a), reacted to both SARS-CoV-2 S6P_{ecto} protein and recombinant
91 soluble NTD protein, whereas the dengue virus mAb DENV-2D22, a negative control for the
92 assays, reacted to neither (**Fig 1A and B**). We performed two types of virus neutralization assays
93 with COV2-2676 and COV2-2489. The first method used authentic WA1/2020 strain SARS-CoV-
94 2 in a focus reduction neutralization test (FRNT) (Harcourt et al., 2020a; Harcourt et al., 2020b),
95 whereas the second was a real-time cell analysis (RTCA) assay using recombinant replication-
96 competent vesicular stomatitis virus (VSV) expressing the SARS-CoV-2 S protein in place of the
97 endogenous VSV glycoprotein (Case et al., 2020b). Both COV2-2676 and COV2-2489
98 individually neutralized the authentic SARS-CoV-2 in a dose-dependent manner with a half-
99 maximal inhibitory (IC₅₀) value of 501 or 199 ng/mL, respectively (**Fig 1C**). In addition, COV2-
100 2676 and COV2-2489 neutralized chimeric VSV-SARS-CoV-2 with IC₅₀ values of 38 or 56
101 ng/mL, respectively (**Fig 1D**).

102 Competition-binding analysis using the S6P_{ecto} protein revealed that COV2-2676 and
103 COV2-2489 competed for binding with one another (**Fig S1**). However, these mAbs did not
104 compete for binding with any of the other 33 previously identified non-neutralizing NTD-reactive
105 human mAbs (Zost et al., 2020b) or with mAbs that recognize non-overlapping antigenic sites on
106 the surface of RBD (including COV2-2196, COV2-2130, and a recombinant form of CR3022(ter
107 Meulen et al., 2006) [**Fig 1E**]). These findings indicate an antigenic site for COV2-2676 and
108 COV2-2489 distinct from those previously identified for neutralizing human mAbs targeting the
109 RBD. Moreover, neither COV2-2676 nor COV2-2489 inhibited the interaction of soluble ACE2
110 with soluble RBD protein (**Fig 1F**).

111 **COV2-2676 and COV2-2489 recognize the NTD of SARS-CoV-2 S protein.** To
112 determine the binding sites for these mAbs, we used negative-stain electron microscopy to image
113 a stabilized trimeric form of the ectodomain of S protein (S6P_{ecto} trimer) in complex with Fab
114 fragment forms of COV2-2676 or COV2-2489 (**Fig 2A**). These antibodies bind to the NTD and
115 recognize the ‘closed’ conformational state of the S6P_{ecto} trimer. By overlaying the negative stain
116 EM maps of the two Fab/S complexes, we determined that these antibodies bind to a common
117 antigenic site on the NTD of the S6P_{ecto} trimer. These findings are consistent with the competition-
118 binding data between COV2-2676 and COV2-2489. Sequence alignment of the variable gene
119 sequences of these mAbs with previously published anti-NTD neutralizing mAbs 4A8 and 4-8
120 showed that COV2-2676 or COV2-2489 are independent clonotypes. COV2-2489 is encoded by
121 heavy chain variable gene segment *IGHV-4-39*. COV2-2676 mAb is encoded by *IGHV1-69*, as is
122 mAb 4-8, but the HCDR3 regions of the two mAbs differ completely, and mAb 4A8 is encoded
123 by *IGHV1-24* (**Table S1**). We superimposed the COV2-2676 negative stain-EM Fab complex with
124 the cryo-EM structure of mAb 4-8 and found that the binding interfaces of both mAbs are similar.

125 The heavy chain of the antibodies interact with the N3 and N5 loops of NTD (**Fig S2**). This
126 revealed a distinct site of vulnerability on NTD region of spike protein for human neutralizing
127 mAbs and suggested a convergent responses in SARS-CoV-2 immune individuals.

128 We next defined the antibody epitopes at the amino acid level using two complementary
129 methods: alanine-scanning loss-of-binding experiments in cell-surface antigen display and
130 selection of virus escape mutants followed by sequence analysis. Screening of the NTD Ala-scan
131 library identified residues A123, G142, Y144, F157 and N164 as important for binding of COV2-
132 2489, and Y144 for binding of mAb COV2-2676. None of these single-residue alanine mutants
133 affected binding of the control NTD-reactive mAb COV2-2305, likely due to the location of key
134 contact residues in the N3 and N5 loops of NTD (**Fig 2B and S3A**).

135 To identify neutralization escape mutations, we used a high-throughput RTCA assay as
136 previously described (Gilchuk et al., 2020a; Gilchuk et al., 2020b). We selected viral variants that
137 escape antibody neutralization at a single saturating concentration of 5 $\mu\text{g}/\text{mL}$ (COV2-2676) or 50
138 $\mu\text{g}/\text{mL}$ (COV2-2489) and identified point mutations. The mutations were F140S (orange) for
139 COV2-2676, and G142D and R158S (green) for COV2-2489 (**Fig 2C**). We confirmed that the
140 mutations in the viral variants we selected in the RTCA assay experiments above conferred
141 resistance to 10 or 100 $\mu\text{g}/\text{mL}$ of the respective mAbs (**Fig S3B**). The location of the escape
142 mutations was in the same region identified by the alanine-scanning method, although the specific
143 amino acids differed between the two methods. Thus, the two neutralizing NTD antibodies bind
144 to a common antigenic site, but the fine specificity of the epitopes differ.

145 **COV2-2676 and COV2-2489 bind avidly to S protein on the surface of infected cells,**
146 **show cell-type specific neutralization, and inhibit at a post-attachment step.** We evaluated the
147 ability of mAbs targeting the NTD to bind to the surface of SARS-CoV-2-infected cells since this

148 property could contribute to immune cell-mediated clearance *in vivo*. Following SARS-CoV-2
149 infection, cells were incubated with serial dilutions of COV2-2489, COV2-2676, the neutralizing
150 RBD-targeting mAb COV2-2381(Zost et al., 2020a), or the dengue virus mAb 2D22 isotype
151 control, prior to analysis of staining intensity by flow cytometry. COV2-2489 and COV2-2676
152 exhibited similar avidity for cell-surface-associated S protein, with EC₅₀ values for staining of
153 infected cells of 896 ng/mL or 1,438 ng/mL, respectively (**Fig 3A**, left panel). Whereas the RBD-
154 targeting mAb COV2-2381 had a more potent EC₅₀ value for binding to infected cells (45 ng/mL),
155 the NTD-targeting mAbs had greater staining intensity of infected cells, as the peak integrated
156 mean fluorescence intensity (iMFI) was higher for COV2-2489 and COV2-2676 than for COV2-
157 2381 (**Fig 3A**, left and right panels, and **Fig S4A**). These data suggest that NTD-targeting mAbs
158 can bind efficiently and at high density to S protein on the surface of SARS-CoV-2 infected cells.

159 We next assessed the neutralizing activity of COV2-2489 and COV2-2676 by FRNT on
160 additional cell lines: MA104 cells, HEK-293T cells ectopically expressing ACE2 (293T+ACE2),
161 and Vero cells ectopically expressing TMPRSS2 (Vero+TMPRSS2), in comparison to wild-type
162 Vero cells. For both mAbs, neutralization potency was greater on Vero cells than MA104 cells or
163 293T+ACE2 cells; both mAbs had weak neutralization potency when assessed using the latter two
164 cell types (**Fig 3B**). TMPRSS2 over-expression did not alter the potency of the mAbs, as
165 neutralization assays using Vero+TMPRSS2 cells had similar potency to the parental wild-type
166 cell (**Fig 3B**). These data indicate that mAbs against the NTD exhibit cell type-dependent
167 neutralization, which may be due to variable expression of entry factors and receptors on the
168 surface of different cell types.

169 To probe further the mechanism of neutralization of mAbs targeting the NTD, we
170 performed modified FRNTs, in which SARS2-CoV-2 was incubated with mAb before (pre-

171 attachment FRNT) or after (post-attachment FRNT) virus was absorbed to the surface of Vero
172 cells. Both COV2-2489 and COV2-2676 efficiently neutralized SARS-CoV-2 when added
173 following virus absorption to the surface of cells (**Fig 3C**). These data suggest that mAbs targeting
174 the NTD can neutralize SARS-CoV-2 at a post-attachment step of the viral life cycle in Vero cells.

175 We also performed experiments that directly assessed the ability of NTD mAbs to block
176 virus attachment to Vero E6 cells and Vero overexpressing hACE2 and TMPRSS2 cells. When
177 hACE2 and TMPRSS2 were expressed in cells ectopically, greater SARS-CoV-2 attachment was
178 observed (**Fig 3D**, left panel). Neither anti-NTD (COV2-2489 or COV2-2676) nor anti-RBD
179 neutralizing mAbs (COV2-2381 or COV2-2196) blocked attachment to Vero E6 cells (**Fig 3D**,
180 middle panels). However, in hACE2 and TMPRSS2 over expressing cells binding was inhibited
181 by anti-RBD but not anti-NTD mAbs (**Fig 3D**, right panels).

182 **COV2-2676 and COV2-2489 require intact IgG or F(ab')₂ for neutralizing activity.**

183 Next, to determine the valency of binding required for activity, we created recombinant IgG,
184 F(ab')₂, and Fab forms of COV2-2676 and COV2-2489 and investigated their neutralizing potency
185 on Vero cells. IgG or F(ab')₂ versions of COV2-2676 or COV2-2489 exhibited neutralizing
186 activity in the RTCA assay, with IC₅₀ values of 0.17 or 0.32 nM (COV2-2676) or 0.28 or 1.20 nM
187 (COV2-2489), respectively (**Fig 3E**). Neutralizing activity of the F(ab')₂ molecules was
188 comparable to that of the IgG versions. However, Fab fragments of COV2-2676 or COV2-2489
189 did not neutralize infection, whereas a potentially neutralizing RBD antibody did inhibit infection as
190 a Fab (**Fig 3E**). The reason for loss of neutralization activity by Fab fragments of COV2-2676 and
191 COV2-2489 is unclear. The larger IgG or F(ab')₂ might sterically hinder functional interactions of
192 the S protein in entry. Alternatively, the monovalent Fab molecule may bind with too low an
193 affinity to the NTD to inhibit entry.

194 **COV2-2676 and COV2-2489 protect against SARS-CoV-2 challenge in mice.** We
195 tested the protective efficacy of COV2-2676 or COV2-2489 monotherapy in a K18-hACE2-
196 transgenic mouse model of SARS-CoV-2 infection (Golden et al., 2020; Oladunni et al., 2020;
197 Winkler et al., 2020). Mice treated with 200 μ g (10 mg/kg) of the isotype control mAb DENV-
198 2D22 one day before intranasal inoculation with 10^3 plaque-forming units (PFU) of SARS-CoV-
199 2 (strain 2019n-CoV/USA_WA1/2020) experienced weight loss between 4 and 7 days after
200 inoculation (**Fig 4A**). In contrast, prophylaxis with 200 μ g of COV2-2676 or COV2-2489
201 prevented weight loss in all mice, in a manner similar to that mediated by COV2-2381, a
202 neutralizing RBD-specific human mAb known to protect *in vivo* against SARS-CoV-2 infection
203 (Zost et al., 2020a). Pre-treatment with COV2-2676 or COV2-2489 also significantly decreased
204 viral burden at 7 days post-infection (dpi) in the upper and lower respiratory tracts and at a distal
205 site, the heart, compared to DENV-2D22, in a manner similar to COV2-2381 (**Fig 4B**).
206 Prophylaxis with 200 μ g of COV2-2676, COV2-2489, or COV2-2381 was associated with serum
207 IgG1 concentrations of ~ 4 μ g/mL (**Fig 4C**). Pre-treatment with COV2-2676 or COV2-2489
208 protected against weight loss and viral burden at a 25-fold lower dose, whereas pre-treatment with
209 COV2-2381 protected at a 125-fold lower dose. These treatments were associated with serum IgG1
210 concentrations of ~ 200 ng/mL or ~ 10 ng/mL, respectively (**Fig 4D-F**). Since SARS-CoV-2
211 infection causes substantial lung inflammation in K18-hACE2 mice and in humans (Golden et al.,
212 2020; Oladunni et al., 2020; Winkler et al., 2020), we evaluated the effects of mAb treatment on
213 cytokine and chemokine production in lung tissues at 7 dpi. Prophylaxis with 200 μ g of COV2-
214 2676 reduced multiple cytokine and chemokine levels in a manner similar to COV2-2381, in
215 contrast with results from the isotype control mAb DENV-2D22 group (**Fig 4G and S5A**).
216 Consistent with these results, analysis of hematoxylin and eosin-stained lung sections showed a

217 reduction in perivascular and parenchymal immune cell infiltration, and alveolar space
218 consolidation in the lungs of COV2-2676 or COV2-2381-treated mice compared to DENV-2D22-
219 treated animals (**Fig 4H**).

220 We next assessed the therapeutic efficacy of monotherapy with COV2-2676 or COV-2489
221 in a post-exposure setting. Mice treated with 200 μ g of COV2-2676 or COV2-2489 one day after
222 SARS-CoV-2 inoculation maintained weight, in a manner similar to COV2-2381 treatment and in
223 contrast to the isotype control mAb, DENV-2D22 (**Fig 5A**). Therapy with COV2-2676 or COV2-
224 2489 also decreased viral burden at 7 dpi in the upper and lower respiratory tract and heart,
225 compared to DENV-2D22, in a manner similar to COV2-2381 (**Fig 5B**). Animals treated with
226 COV2-2676 also had lower levels of multiple cytokines and chemokines in lung homogenates,
227 similar to COV2-2381 and in contrast to DENV-2D22 (**Fig 5C and S5B**). Pathological analysis
228 also showed less immune cell infiltration and airspace consolidation after COV2-2676 or COV2-
229 2381 therapy compared to DENV-2D22 treatment (**Fig 5D**).

230 **Fc effector functions contribute to optimal protection by COV2-2676 or COV-2489.**
231 Because the NTD mAbs bound avidly to the surface of SARS-CoV-2-infected cells (**Fig 3A and**
232 **S4A**), we speculated that part of their protective activity might be mediated by effector functions
233 through Fc engagement of C1q or Fc γ Rs that could promote clearance. To test this hypothesis, we
234 engineered LALA-PG mutations into the Fc region of these human IgG1 mAbs to abrogate
235 interaction of the Fc region with Fc γ Rs and complement proteins (Lund et al., 1991; Wines et al.,
236 2000). We confirmed that the LALA-PG mutations in COV2-2676 and COV2-2489 did not affect
237 S protein binding (**Fig S4B**) or neutralizing activity (**Fig S4C**).

238 We then evaluated if the LALA-PG Fc variants lost protective activity *in vivo*. Despite
239 similar concentrations in serum at the time of SARS-CoV-2 infection (**Fig 4C**), increased weight

240 loss and viral burden, as well as greater lung inflammation and pathology were observed in animals
241 pre-treated with COV2-2676 LALA-PG Fc or COV2-2489 LALA-PG Fc variant IgGs compared
242 to the intact parental mAbs (**Fig 4A, B, E, G, and H**). This pattern also was seen with therapy
243 initiated one day after SARS-CoV-2 infection using COV2-2676 LALA-PG Fc or COV2-2489
244 LALA-PG Fc variants (**Fig 5A-D**). Overall, these findings suggest that Fc effector function
245 activities contribute to the protection conferred by each of the NTD mAbs.

246 The combination of an RBD-specific neutralizing mAb and an NTD mAb in a cocktail
247 would confer equivalent or better levels of protection, since binding to distinct antigenic sites
248 might mitigate the risk of selection of antibody escape variants. Thus, mAb cocktails that include
249 components binding to different epitopes on S protein offer higher resistance to escape mutations
250 (Baum et al., 2020b; Greaney et al., 2021) and protect animals from SARS-CoV-2 challenge
251 (Baum et al., 2020a; Zost et al., 2020a). Initially, to test this approach, we used VSV expressing
252 escape variants of the SARS-CoV-2 S protein that were resistant to neutralization by RBD-specific
253 antibodies (COV-2479 or COV2-2130) (Greaney et al., 2021) and the NTD-specific antibodies
254 described here (COV2-2676 and COV2-2489). As expected, NTD-reactive mAbs neutralized the
255 RBD mAb escape mutant viruses, and RBD-reactive mAbs neutralized the NTD mAb escape
256 mutant viruses (**Fig 6A**).

257 We next treated mice two days after inoculation with SARS-CoV-2 with individual mAbs
258 or a combination of COV2-2381 (RBD-specific) and COV2-2676 (NTD-specific) mAbs. Mice
259 treated with 200 µg of COV2-2676, COV2-2489 or COV2-2831 two days after SARS-CoV-2
260 inoculation showed weight loss, viral burden, and inflammatory mediator profiles that were similar
261 to DENV-2D22-treated mice (**Fig 6B-D**), consistent with a limited therapeutic window for
262 effective treatment in this stringent transgenic hACE2 mouse model. While mice were not

263 protected from the initial phase of weight loss, viral infection in the lower respiratory tract or heart,
264 or lung inflammation (**Fig 6B-D, S5C**), treatment with mAb monotherapy or the cocktail resulted
265 in weight gain beginning approximately one week after infection and survival through two weeks
266 after infection, and this recovery was associated with decreased nasal wash titers and reduced lung
267 pathology (**Fig 6B-D**). In comparison, all mice treated with the isotype control mAb DENV-2D22
268 had severe lung pathology and succumbed to infection between eight and nine days after
269 inoculation. These results suggested that diversification of neutralizing antibody responses after
270 natural infection or vaccination (*e.g.*, targeting of vulnerable RBD and NTD sites of the spike)
271 could be beneficial for protective immunity, with a potential implication for therapeutic cocktail
272 design.

273 **DISCUSSION**

274 Several research groups have identified RBD-specific mAbs using B cells from SARS-
275 CoV-2 convalescent individuals, with a number of these mAbs now in Phase III clinical trials
276 (Baum et al., 2020a; Chen et al., 2020a; Jones et al., 2020) and two mAb products having obtained
277 Emergency Use Authorization from the U.S. Food and Drug Administration. Due to the large
278 number of natural variant viruses with polymorphisms in the RBD that are emerging, identification
279 of neutralizing and protective human mAbs that bind to other antigenic sites on the S protein is
280 warranted. In a large (n =389) panel of mAbs we isolated with reactivity to the SARS-CoV-2 S
281 protein, the majority of mAbs bound to S protein but not to the RBD (Zost et al., 2020b). We found
282 that a small subset of non-RBD antibodies that recognized the NTD could neutralize SARS-CoV-
283 2 infection and confer protection in a stringent hACE2 transgenic mouse model of disease.

284 Our studies highlight the promising functional activities of NTD-specific mAbs. Although
285 these mAbs did not bind as avidly to recombinant S6P_{ecto} protein as did the most potent RBD-
286 reactive mAbs we isolated, they neutralized SARS-CoV-2 with potencies comparable to many
287 RBD-targeting antibodies (Zost et al., 2020a; Zost et al., 2020b). Very few NTD-targeting
288 neutralizing antibodies have been reported to date. Sequence comparison of recently published
289 NTD-reactive SARS-CoV-2 mAbs 4A8 (Chi et al., 2020) and 4-8 (Liu et al., 2020a) revealed that
290 our mAbs are genetically distinct and not members of a public clonotype matching those mAbs
291 (**Table S1**).

292 Most neutralizing SARS-CoV-2 mAbs block RBD interactions with ACE2 (Brouwer et
293 al., 2020; Cao et al., 2020; Ju et al., 2020; Liu et al., 2020a; Rogers et al., 2020; Seydoux et al.,
294 2020; Wec et al., 2020; Wu et al., 2020; Zost et al., 2020a; Zost et al., 2020b). However, the
295 mechanism of neutralization of NTD-reactive antibodies appears complex. Our data suggest that

296 the anti-NTD antibodies COV2-2676 and COV2-2489 inhibit at a post-attachment phase of
297 infection and may block subsequent virus entry or fusion steps. In cells in which anti-RBD and
298 anti-NTD antibodies do not appear to block virus attachment (*i.e.*, conventional Vero cells), both
299 groups inhibited at a post-attachment step. Virus attachment to cells can differ in diverse cells,
300 likely because of the capacity of SARS-CoV-2 to use multiple attachment factors including
301 heparan sulfates, hACE2, TAM receptors, and possibly other molecules (Cantuti-Castelvetri et al.,
302 2020; Chen et al., 2020b; Chiodo et al., 2020; Clausen et al., 2020; Gao and Zhang, 2020). The
303 mechanism of attachment in Vero (monkey kidney) cells without human ACE2 transfection is
304 uncertain; attachment might be mediated by monkey ACE2 although this has not been formally
305 demonstrated. It is possible that the NTD antibodies block entry by indirectly interfering with
306 ACE2 binding through steric interference of the Fc region. In analogous experiments with MERS-
307 CoV, structural studies presented showed that the MERS-CoV mAb 7D10 could bind to the NTD
308 of S protein of MERS-CoV and inhibit RBD-DPP4 interaction through its light chain, which was
309 close to the RBD (Zhou et al., 2019). We tested that model here but found that neither COV2-2676
310 nor COV2-2489 blocked ACE2 interaction with RBD in soluble protein or in cell-surface-display
311 assays. Antibody fragment studies using Fab, F(ab')₂ and IgG forms of COV2-2676 and COV2-
312 2489 showed that the Fab forms lost neutralizing activity, possibly suggesting some blocking
313 occurs indirectly by steric effects of the projecting Fc region into the direction of the RBD as in
314 the case for the MERS-CoV mAb 7D10 (Zhou et al., 2019). However, we did not obtain direct
315 evidence for this mechanism. In cells expressing high hACE2 levels, anti-RBD antibodies partially
316 inhibited attachment of virus, but anti-NTD antibodies did not.

317 To define the fine specificity of this protective epitope, we performed saturation alanine-
318 scanning mutagenesis studies and identified critical residues for binding of COV2-2676 or COV2-

319 2489 mAbs in the NTD. We showed that SARS-CoV-2 S protein variants with mutations at F140S
320 and G142D, or R158S in the NTD conferred resistance to COV2-2676 or COV2-2489,
321 respectively, using a chimeric replication-competent VSV expressing the SARS-CoV-2 S protein.
322 Consistent with these data, Weisblum *et al.* identified an NTD epitope (residues 148 to 151), and
323 mutations in this epitope enabled escape from neutralizing antibody activity in a donor plasma
324 specimen (Weisblum *et al.*, 2020).

325 We first tested the prophylactic efficacy of COV2-2676 or COV2-2489 in a well-defined
326 model of SARS-CoV-2 infection in hACE2-expressing transgenic mice (Winkler *et al.*, 2020).
327 Mice pre-treated with COV2-2676 or COV2-2489 mAbs exhibited substantially lower viral titers
328 than mice treated with an isotype-control mAb and offered complete protection against death in
329 this model. We also assessed the therapeutic potential of these mAbs in the same mouse model.
330 Each of the mAbs mediated a therapeutic effect when administered after infection. Although
331 several protection studies of anti-SARS-CoV-2 mAbs have been published, all of these
332 experiments used mAbs directed against the RBD (Baum *et al.*, 2020a; Chen *et al.*, 2020a; Hassan
333 *et al.*, 2020; Wang *et al.*, 2020; Zost *et al.*, 2020a). There is only limited precedence for *in vivo*
334 protection against SARS-CoV-2 infection or disease mediated by mAbs that react to S protein
335 regions outside the RBD (McCallum *et al.*, 2021; Voss *et al.*, 2020; Zhang *et al.*, 2020).

336 IgG interactions with Fc γ receptors and complement contribute to antibody-dependent viral
337 clearance during many infections, including HIV-1, Ebola, influenza, and chikungunya viruses
338 (DiLillo *et al.*, 2014; Fox *et al.*, 2019; Halper-Stromberg *et al.*, 2014; Lu *et al.*, 2016). MAbs against
339 SARS-CoV-1 and SARS-CoV-2 also can confer protective effects in part through through Fc-
340 mediated effector functions (Atyeo *et al.*, 2020; Pinto *et al.*, 2020; Schafer *et al.*, 2021). To test
341 whether this was the case with our mAbs, we generated COV2-2676 and 2489 LALA-PG variant

342 Fc versions. Indeed, Fc-mediated activity for NTD-specific mAbs did contribute to protection in
343 the models we tested. Animals in the LALA-PG mAb-treated mice groups had increased viral
344 burden and lost weight, but still survived viral challenge, suggesting involvement of Fc-effector
345 function dependent and independent mechanisms in the protection *in vivo* conferred by anti-NTD
346 mAbs.

347 SARS-CoV-2 continues to evolve, and its capacity to escape the activity of neutralizing
348 antibodies in current clinical development is not fully understood. The emergence of mutations at
349 E484K in South African strains is concerning, because this change can impact the neutralizing
350 activity of many RBD-specific mAbs and immune serum generated from convalescent subjects
351 (Avanzato et al., 2020; Greaney et al., 2021; Liu et al., 2020b; Oude Munnink et al., 2021; Piccoli
352 et al., 2020; Rambaut et al., 2020; Starr et al., 2020). Moreover, the administration of convalescent
353 plasma with suboptimal levels of neutralizing antibodies might increase resistance in circulating
354 SARS-CoV-2 populations (Bloch, 2020). Furthermore, candidate vaccines that include only RBD
355 antigens lack the ability to induce NTD-reactive neutralizing antibodies (Laczko et al., 2020;
356 Mulligan et al., 2020; Smith et al., 2020; Yu et al., 2020). Antibody therapy or vaccine approaches
357 that target additional antigenic sites may limit escape and prevent compromising of vaccine- or
358 natural infection-induced immunity. A combination of RBD- and NTD-reactive neutralizing mAbs
359 may offer an attractive alternative approach to treatments that target only RBD. The data presented
360 here describing neutralization escape viruses suggests the potential utility of using mAb cocktails
361 to avoid selection of neutralization resistant viruses. Moreover, we establish that a combination of
362 RBD- and NTD-reactive neutralizing mAbs can be used as an effective therapeutic cocktail *in*
363 *vivo*. Overall, the results presented here provide compelling evidence that some NTD-targeting

364 mAbs can inhibit SARS-CoV-2 infection efficiently *in vitro* and *in vivo*, using both neutralizing
365 and Fc-mediated effector function activities.
366

367 **ACKNOWLEDGEMENTS**

368 We thank Ryan Irving at Vanderbilt University Medical Center for laboratory management
369 support and Merissa Mayo and Norma Suazo Galeano for human subjects support. EM data
370 collections were conducted at the Center for Structural Biology Cryo-EM Facility at Vanderbilt
371 University. This work was supported by the NIAID/NIH grants T32 AI095202 (S.J.Z.), T32
372 AI007163 (E. S. W.), and R01 AI157155 (M.S.D. and J.E.C.), HHSN contracts 75N93019C00074
373 (J.E.C.) and 75N93019C00073 (B.J.D.), DARPA HR0011-18-2-0001 (J.E.C.); the Dolly Parton
374 COVID-19 Research Fund at Vanderbilt (J.E.C.); and Fast Grants, Mercatus Center, George
375 Mason University (J.E.C.). J.E.C. is a recipient of the 2019 Future Insight Prize from Merck
376 KGaA. The content is solely the responsibility of the authors and does not represent the official
377 views of the U.S. government or other sponsors.

378

379 **AUTHOR CONTRIBUTIONS**

380 Conceived of the project: N.S., P.G., S.J.Z., R.H.C., L.B.T., M.S.D., J.E.C.; Obtained
381 funding: M.S.D. and J.E.C. Performed laboratory experiments: N.S., S.S., P.G., E.S.W., E.B.,
382 S.J.Z., L.V., R.S.N., R.E.S., S.P.K., M.E.F., L.B.T. Performed computational work: E.C.C.
383 Supervised research: R.H.C., L.B.T., E.D., B.D., M.S.D., J.E.C. Wrote the first draft of the paper:
384 N.S., P.G., S.S., L.B.T., M.S.D., J.E.C.; All authors reviewed and approved the final manuscript.

385

386 **DECLARATION OF INTERESTS**

387 M.E.F., E.D., and B.J.D. are employees of Integral Molecular. B.J.D. is a shareholder of
388 Integral Molecular. M.S.D. is a consultant for Inbios, Vir Biotechnology, NGM
389 Biopharmaceuticals, and Carnival Corporation, is on the Scientific Advisory Boards of Moderna

390 and Immunome, and the Diamond laboratory at Washington University School of Medicine has
391 received sponsored research agreements from Emergent BioSolutions, Moderna, and Vir
392 Biotechnology. J.E.C. has served as a consultant for Eli Lilly, GlaxoSmithKline and Luna
393 Biologics, is a member of the Scientific Advisory Boards of CompuVax and Meissa Vaccines and
394 is Founder of IDBiologics. The Crowe laboratory at Vanderbilt University Medical Center has
395 received unrelated sponsored research agreements from IDBiologics and AstraZeneca.
396

397 **FIGURE LEGENDS**

398

399 **Figure 1. Two non-RBD-reactive mAbs specific to SARS-CoV-2 S protein neutralize the**
400 **virus.**

401 **A.** ELISA binding of COV2-2196, COV2-2263, COV2-2489, COV2-2490, COV2-2676 or
402 rDENV-2D22 to trimeric S-6P_{ecto}. Data are mean \pm standard deviations (S.D.) of technical
403 triplicates from a representative experiment repeated twice.

404 **B.** ELISA binding of COV2-2196, COV2-2263, COV2-2489, COV2-2490, COV2-2676 or
405 rDENV-2D22 to rNTD protein. Data are mean \pm S.D. of technical triplicates from a representative
406 experiment repeated twice.

407 **C.** Neutralization curves for COV2-2196, COV2-2489, COV2-2676 or rDENV-2D22 using wild-
408 type SARS-CoV-2 in a FRNT assay. Error bars indicate S.D.; data represent at least two
409 independent experiments performed in technical duplicate.

410 **D.** Neutralization curves for COV2-2196, COV2-2489, COV2-2490, COV2-2676 or rDENV-
411 2D22 in a SARS-CoV-2-rVSV neutralization assay using RTCA. Error bars indicate S.D.; data
412 are representative of at least two independent experiments performed in technical duplicate.

413 **E.** Competition binding of the panel of neutralizing mAbs with reference mAbs COV2-2130,
414 COV2-2196, COV2-2263, COV2-2489, COV2-2676 or rCR3022. Binding of reference mAbs to
415 trimeric S-6P_{ecto} protein was measured in the presence of saturating concentration of competitor
416 mAb in a competition ELISA and normalized to binding in the presence of rDENV-2D22. Black
417 indicates full competition (<25% binding of reference antibody); grey indicates partial competition
418 (25 to 60% binding of reference antibody); white indicates no competition (>60% binding of
419 reference antibody).

420 **F.** Human-ACE2-blocking curves for COV2-2196, COV2-2263, COV2-2489, COV2-2490,
421 COV2-2676 and rDENV-2D22 in a human-ACE2-blocking ELISA. Data are mean \pm S.D. of
422 technical triplicates from a representative experiment repeated twice.

423

424 **Figure 2. COV2-2676 and COV2-2489 binding map to the NTD of SARS-COV-2-S protein.**

425 **A.** Top row (side view), bottom row (top view) of Fab–S6Pecto closed trimer (S protein model
426 PDB:7JJI) complexes visualized by negative-stain electron microscopy for COV2-2676 Fab model
427 in pink, COV2-2489 Fab model in blue and superimpose 3D volume of CoV2-S-Fab 2676 complex
428 in grey and CoV2-S-Fab 2489 in mesh. The S-NTD is shown in yellow and electron density in
429 grey. Representative two-dimensional (2D) class averages for each complex are shown at the
430 bottom (box size is 128 pixels, with 4.36 Å per pixel). Data are from a single experiment; detailed
431 collection statistics are provided in **Supplementary Table 2**.

432 **B.** Identification of critical contact residues by alanine-scanning mutagenesis. Top (side view) with
433 loss of binding residues (cyan) for COV2-2489 or COV2-2676 to mutant S-NTD constructs,
434 normalized to the wild-type. Bottom, escape mutations mapped to the NTD region for COV2-2489
435 (green G142D, R158S) or COV2-2676 (orange F140S). **C.** Results of viral selections with COV2-
436 2489 or COV2-2676 individual mAbs. The number of replicates in which escape variants were
437 selected is indicated. Mutations present in the NTD of the selected escape variants are indicated.

438

439 **Figure 3. Virus neutralization and binding of infected cells by anti-SARS-CoV-2 mAbs**
440 **targeting the NTD.** **A.** SARS-CoV-2-infected Vero cells were stained with serial dilutions of
441 COV2-2489, COV2-2676, COV2-2381, or DENV2-2D22 (isotype control) prior to analysis of
442 staining intensity by flow cytometry. The positively stained cells were gated using uninfected and

443 isotype control mAb-stained infected cells, and the integrated mean fluorescence intensity (iMFI)
444 was determined by MFI of positive cells multiplied by the percent of total positive cells. The left
445 panel shows representative dose response curves for the staining intensity of infected cells by each
446 mAb. The right panel shows the mean EC₅₀ values for infected cell staining, determined from three
447 independent experiments. Error bars represent SEM.

448 **B-D.** The neutralization potency of COV2-2489 and COV2-2676 against SARS-CoV-2 was
449 assessed by FRNT using **(B)** Vero, MA104, 293T+ACE2, and Vero+TMPRSS2 cells. Results are
450 representative of three independent experiments performed in duplicate. **(C)** COV2-2489 and
451 COV2-2676 were assayed for neutralization potency by modified FRNT in which mAb was added
452 to SARS-CoV-2 before (pre-attachment, filled circles) or after (post-attachment, open circles)
453 virus was absorbed to Vero E6 cells. **(C)** Error bars represent the range from two technical
454 replicates. Data shown are representative of three independent experiments. **D.** Attachment
455 inhibition. *(Left panel)* Vero or Vero+hACE2+TMPRSS2 cells were incubated with SARS-CoV-
456 2 at 4°C for 1 h. After extensive washing, cell-bound viral RNA was measured by qRT-PCR. *(Right*
457 *4 panels)* SARS-CoV-2 was pre-incubated with 5 or 50 µg/mL of indicated anti-RBD or anti-NTD
458 mAbs for 1 h prior to addition to Vero or Vero+hACE2+TMPRSS2 cells. Cell-bound viral RNA
459 was measured by qRT-PCR. Data are pooled from three independent experiments. *(Left)* t-test:
460 ****p<0.0001; *(Right)* One-way ANOVA with Dunnett's multiple comparisons test compared to
461 isotype control mAb treatment: *p<0.05; **p<0.01; ***p<0.001. **E.** Neutralization curves for
462 COV2-2196 IgG, F(ab')₂, F(ab) or rDENV-2D22; COV2-2489 IgG, F(ab')₂, F(ab); or COV2-2676
463 IgG, F(ab')₂, F(ab) in a SARS-CoV2-rVSV assay using RTCA. Error bars indicate S.D.; data
464 represent at least two independent experiments performed in technical triplicates.

465

466 **Figure 4. Prophylaxis with COV2-2676 or COV2-2489 confers protection against SARS-**
467 **CoV-2 in mice.**

468 Eight to nine week-old male and female K18 hACE2 transgenic mice were administered by
469 intraperitoneal (i.p.) injection 200, 40, 8 or 1.6 μ g of COV2-2676, COV2-2489, COV2-2676
470 LALA-PG, COV2-2489 LALA-PG, COV2-2381 (a positive control) or DENV-2D22, an isotype
471 control, mAb a day before virus inoculation (D-1). One day later, mice were inoculated intranasally
472 (i.n.) with 10^3 PFU of SARS-CoV-2.

473 **A.** Body weight change of mice over time. Data shows the mean \pm S.E.M. compared to the isotype
474 control mAb for two independent experiments (n = 6 to 11 for each experimental group; one-
475 way ANOVA with Dunnett's post hoc test of area under the curve from 4 to 7 dpi: ns, not
476 significant, **p < 0.01, ****p < 0.0001).

477 **B.** Tissues were harvested at 7 dpi from a subset of mice in **A**. Viral burden in the lung, nasal
478 wash, and heart was assessed by qRT-PCR of the N gene. Data shows the mean \pm S.E.M.
479 compared between all groups for two independent experiments (n = 6 for each experimental
480 group; one-way ANOVA with Tukey's post hoc test: ns, not significant, *p < 0.05, **p < 0.01,
481 ***p < 0.001, ****p < 0.0001). Dashed line represents limit of detection of assay.

482 **C.** Serum concentration (ng/ml) of human mAbs at the time of SARS-CoV-2 infection of the mice
483 in **B**. Data shows the mean \pm S.E.M. compared between all groups for two independent
484 experiments (n = 6 for each experimental group; one-way ANOVA with Tukey's post hoc test:
485 ns, not significant, ****p < 0.0001).

486 **D.** Body weight change of mice over time. Data shows the mean \pm S.E.M. compared to isotype
487 control mAb for two independent experiments (n = 4 to 8 for each experimental group; one-

488 way ANOVA with Dunnett's post hoc test of area under the curve from 4 to 7 dpi: ns, not
489 significant, *** $p < 0.001$, **** $p < 0.0001$).

490 **E.** Tissues were harvested at 7 dpi from mice in **D**. Viral burden in the lung, nasal wash, and heart
491 was assessed by qRT-PCR of the N gene. Data shows the mean \pm S.E.M. compared between
492 all groups for two independent experiments ($n = 4$ to 8 for each experimental group; one-way
493 ANOVA with Tukey's post hoc test: ns, not significant, * $p < 0.05$, ** $p < 0.01$, *** $p <$
494 0.001 , **** $p < 0.0001$).

495 **F.** Serum concentration (ng/mL) of human mAbs at the time of SARS-CoV-2 infection of the
496 mice in **D**. Data shows the mean \pm S.E.M. compared to isotype control mAb at various doses
497 of mAb for two independent experiments ($n = 6$; one-way ANOVA with Dunnett's post hoc
498 test: ns, not significant).

499 **G.** Heat map of cytokine and chemokine levels in lung tissue homogenates harvested in **B** as
500 measured by a multiplex platform. Log₂ fold change compared to lungs from mock-infected
501 animals was plotted in the corresponding heat map (associated statistics are reported in **Fig**
502 **S6A**).

503 **H.** Hematoxylin and eosin staining of lung sections harvested at 7 dpi from mice in **B**. Images are
504 low (top; scale bars, $500 \mu\text{m}$) and high power (bottom; scale bars, $50 \mu\text{m}$). Representative
505 images are shown from two independent experiments ($n = 3$).

506

507 **Figure 5. Therapeutic activity of COV2-2676 or COV-2489 after SARS-CoV-2 challenge.**

508 Eight to nine week-old male and female K18 hACE2 transgenic mice were inoculated with 10^3
509 PFU of SARS-COV2. One day later (D+1), mice were given an i.p. administration of $200 \mu\text{g}$ of

510 COV2-2676, COV2-2489, COV2-2676 LALA PG, COV2-2489 LALA PG, COV2-2381 (a
511 positive control) or DENV-2D22, an isotype control, mAb.

512 **A.** Body weight change of mice over time. Data shows the mean \pm S.E.M. compared to isotype
513 control mAb for two independent experiments (n = 6 to 11 for each experimental group; one-
514 way ANOVA with Dunnett's post hoc test of area under the curve from 4 to 7 dpi: ns, not
515 significant, **p < 0.01, ***p < 0.001, ****p < 0.0001).

516 **B.** Tissues were harvested at 7 dpi from a subset of mice in **A**. Viral burden in the lung, nasal
517 wash, and heart was assessed by qRT-PCR of the N gene. Data shows the mean \pm S.E.M.
518 compared between all groups for two independent experiments (n = 6 to 7 for each
519 experimental group; one-way ANOVA with Tukey's post hoc test: ns, not significant, *p <
520 0.05, **p < 0.01, ***p < 0.001, ****p < 0.0001).

521 **C.** Heat map of cytokine and chemokine levels in lung homogenates harvested in **B** as measured
522 by a multiplex platform. Log₂ fold change compared to lungs from mock-infected animals was
523 plotted in the corresponding heat map (associated statistics are reported in **Fig S6B**).

524 **D.** Hematoxylin and eosin staining of lung sections harvested at 7 dpi from mice in **B**. Images are
525 low (top; scale bars, 500 μ m) and high power (bottom; scale bars, 50 μ m). Representative
526 images are shown from two independent experiments (n = 3).

527

528 **Figure 6. Rationale for design of an antibody cocktail targeting both RBD and NTD**

529 **A.** Neutralization matrix of RBD mAbs (COV2-2479 and COV2-2130 shown in purple) and NTD
530 mAb (COV2-2676 in orange and COV2-2489 in green) escape viruses. Black = full neutralization,
531 grey = partial neutralization, white = no neutralization & * indicates escape viruses that were
532 isolated in previously published study. Eight to nine week-old male or female K18 hACE2

533 transgenic mice were inoculated intranasally with 10^3 PFU of SARS-CoV2. Two days later (D+2),
534 mice were given an i.p. administration of 200 μ g of COV2-2676, COV2-2489, COV2-2676
535 LALA-PG, COV2-2489 LALA-PG, COV2-2381 (a positive control) or DENV-2D22, an isotype
536 control, mAb for monotherapy or 100 μ g each of COV2-2381 and COV2-2676 for combination
537 therapy.

538 **B.** (Left panel) Body weight change of mice over time. Data shows the mean \pm S.E.M. compared
539 to isotype control mAb for two independent experiments (n = 6 to 14 for each experimental group:
540 one-way ANOVA with Dunnett's post hoc test of area under the curve from 4 to 7 dpi. Significant
541 differences were not detected. (Right panel) Percent survival of mice over time. Survival was
542 compared to isotype control for two independent experiments (n = 6 to 14 for each experimental
543 group; log-rank Mantel-Cox test; ****p < 0.0001).

544 **C.** Tissues were harvested at 7 dpi mice from a subset of mice in **B**. Viral burden in the lung, nasal
545 wash, and heart was assessed by qRT-PCR of the N gene. Data shows the mean \pm S.E.M. compared
546 between all groups for two independent experiments: n = 6 to 8 for each experimental group; one-
547 way ANOVA with Tukey's post hoc test: ns, not significant, *p < 0.05, ***p < 0.001).

548 **D.** Heat map of cytokine and chemokine levels in lung homogenates harvested in **C** as measured
549 by a multiplex platform. Log₂ fold change compared to lungs from mock-infected animals was
550 plotted in the corresponding heat map (associated statistics are reported in **Fig S6C**.)

551 **E.** Hematoxylin and eosin staining of lung sections harvested at 7 dpi from mice in **B**. Images are
552 low (top; scale bars, 500 μ m) and high power (bottom; scale bars, 50 μ m). Representative images
553 are shown from two independent experiments (n = 3).

554

555 **STAR METHODS**

556

557 **RESOURCE AVAILABILITY**

558 **LEAD CONTACT.** Further information and requests for resources and reagents should be
559 directed to and will be fulfilled by the Lead Contact, James E. Crowe, Jr. (james.crowe@vumc.org).

560 **MATERIALS AVAILABILITY.** Materials described in this paper are available for
561 distribution for nonprofit use using templated documents from Association of University
562 Technology Managers “Toolkit MTAs”, available at: [https://autm.net/surveys-and-](https://autm.net/surveys-and-tools/agreements/material-transfer-agreements/mta-toolkit)
563 [tools/agreements/material-transfer-agreements/mta-toolkit](https://autm.net/surveys-and-tools/agreements/material-transfer-agreements/mta-toolkit).

564 **DATA AND CODE AVAILABILITY.** All data needed to evaluate the conclusions in the
565 paper are present in the paper or the Supplemental Information. The antibodies in this study are
566 available by Material Transfer Agreement with Vanderbilt University Medical Center.

567

568 **EXPERIMENTAL MODEL AND SUBJECT DETAILS**

569

570 **Antibodies.** The human antibodies studied in this paper were isolated from blood samples from
571 two individuals in North America with previous laboratory-confirmed symptomatic SARS-CoV-
572 2 infection that was acquired in China. The original clinical studies to obtain specimens after
573 written informed consent were previously described (Zost et al., 2020b) and approved by the
574 Institutional Review Board of Vanderbilt University Medical Center, the Institutional Review
575 Board of the University of Washington and the Research Ethics Board of the University of
576 Toronto. The individuals (a 56-year-old male and a 56-year-old female) are a married couple and
577 residents of Wuhan, China who travelled to Toronto, Canada, where PBMCs were obtained by

578 leukopheresis 50 days after symptom onset. The antibodies were isolated using diverse tools for
579 isolation and cloning of single antigen-specific B cells and the antibody variable genes that encode
580 mAbs (Zost et al., 2020b).

581
582 **Cell lines.** Vero E6 (ATCC, CRL-1586), Vero (ATCC, CCL-81), HEK293 (ATCC, CRL-1573) and
583 HEK293T (ATCC, CRL-3216) cells were maintained at 37°C in 5% CO₂ in Dulbecco's minimal
584 essential medium (DMEM) containing 10% (v/v) heat-inactivated fetal bovine serum (FBS), 10 mM
585 HEPES pH 7.3, 1 mM sodium pyruvate, 1× non-essential amino acids and 100 U/mL of penicillin–
586 streptomycin. Vero-furin cells were obtained from T. Pierson (NIAID, NIH) and have been described
587 previously (Mukherjee et al., 2016). Vero-hACE2-TMPRSS2 cells were a gift of A. Creanga and B.
588 Graham (Vaccine Research Center, NIH). FreeStyle 293F cells (Thermo Fisher Scientific, R79007)
589 were maintained at 37°C in 8% CO₂. Expi293F cells (Thermo Fisher Scientific, A1452) were
590 maintained at 37°C in 8% CO₂ in Expi293F Expression Medium (Thermo Fisher Scientific,
591 A1435102). ExpiCHO cells (Thermo Fisher Scientific, A29127) were maintained at 37°C in 8%
592 CO₂ in ExpiCHO Expression Medium (Thermo Fisher Scientific, A2910002). Authentication analysis
593 was not performed for the cell lines used. Mycoplasma testing of Expi293F and ExpiCHO cultures
594 was performed on a monthly basis using a PCR-based mycoplasma detection kit (ATCC, 30-1012K).

595
596 **Viruses.** SARS-CoV-2 strain 2019 n-CoV/USA_WA1/2020 was obtained from the Centers for
597 Disease Control and Prevention (a gift from N. Thornburg). Virus was passaged in Vero CCL81 cells
598 and titrated by plaque assay on Vero E6 cell culture monolayers as previously described (Case et al.,
599 2020a). The generation of a replication-competent VSV expressing SARS-CoV-2 S protein with a 21
600 amino-acid C-terminal deletion that replaces the VSV G protein (VSV-SARS-CoV-2) was described

601 previously (Case et al., 2020b). The S protein-expressing VSV virus was propagated in MA104 cell
602 culture monolayers (African green monkey, ATCC CRL-2378.1) as described previously (Case *et al.*,
603 2020), and viral stocks were titrated on Vero E6 cell monolayer cultures. VSV plaques were visualized
604 using neutral red staining. All work with infectious SARS-CoV-2 was performed in Institutional
605 Biosafety Committee approved BSL3 and A-BSL3 facilities at Washington University School of
606 Medicine using appropriate positive pressure air respirators and protective equipment.

607
608 **Mouse models.** Animal studies were carried out in accordance with the recommendations in the Guide
609 for the Care and Use of Laboratory Animals of the National Institutes of Health. The protocols were
610 approved by the Institutional Animal Care and Use Committee at the Washington University School
611 of Medicine (assurance number A3381–01). Virus inoculations were performed under anesthesia that
612 was induced and maintained with ketamine hydrochloride and xylazine, and all efforts were made to
613 minimize animal suffering. Heterozygous K18-hACE c57BL/6J mice (strain: 2B6.Cg-Tg(K18-
614 ACE2)2Prlmn/J) were obtained from Jackson Laboratory (034860). Eight to nine week-old mice of
615 both sexes were inoculated with 10^3 PFU of SARS-CoV-2 by an intranasal route.

616

617 **METHOD DETAILS**

618

619 **Recombinant antigens and proteins.** A gene encoding the ectodomain of a pre-fusion
620 conformation-stabilized SARS-CoV-2 S protein ectodomain (S6P_{ecto}) (Hsieh et al., 2020) was
621 synthesized and cloned into a DNA plasmid expression vector for mammalian cells. A similarly
622 designed S protein antigen with two prolines and removal of the furin cleavage site for stabilization
623 of the prefusion form of S (S2P_{ecto}) was reported previously (Wrapp et al., 2020). In brief, this

624 gene includes the ectodomain of SARS-CoV-2 (to residue 1,208), a T4 fibrin trimerization
625 domain, an AviTag site-specific biotinylation sequence and a C-terminal 8× His tag. To stabilize
626 the construct in the pre-fusion conformation, we included substitutions F817P, A892P, A899P,
627 A942P, K986P and V987P and mutated the furin cleavage site at residues 682–685 from RRAR
628 to ASVG. The recombinant S6P_{ecto} protein was isolated by metal affinity chromatography on
629 HisTrap Excel columns (Cytiva), and protein preparations were purified further by size-exclusion
630 chromatography on a Superose 6 Increase 10/300 column (Cytiva). The presence of trimeric, pre-
631 fusion conformation S protein was verified by negative-stain electron microscopy (Zost et al.,
632 2020b). For electron microscopy with S protein and Fabs, we expressed a variant of S6P_{ecto} lacking
633 an AviTag but containing a C-terminal Twin-Strep-tag, similar to that described previously (Zost
634 et al., 2020b). Expressed protein was isolated by metal affinity chromatography on HisTrap Excel
635 columns (Cytiva), followed by further purification on a StrepTrap HP column (Cytiva) and size-
636 exclusion chromatography on TSKgel G4000SWXL (TOSOH). To express the RBD subdomain
637 of the SARS-CoV-2 S protein, a synthetic DNA (Twist Bioscience) encoding residues 319–541
638 was cloned into a mammalian expression vector downstream of an IL-2 signal peptide and
639 upstream of a thrombin cleavage site, an AviTag and a 6× His tag. Recombinant SARS-CoV-2 S
640 NTD protein was kindly provided by P. McTamney, K. Ren and A. Barnes (AstraZeneca). Purified
641 proteins were analyzed by SDS–PAGE to ensure purity and appropriate molecular weights.

642

643 **MAb production and purification.** Sequences of mAbs that had been synthesized (Twist
644 Bioscience) and cloned into an IgG1 monocistronic expression vector (designated as pTwist-
645 mCis_G1) or Fab expression vector (designated as pTwist-mCis_FAB) were used for production
646 in mammalian cell culture. This vector contains an enhanced 2A sequence and GSG linker that

647 allows the simultaneous expression of mAb heavy and light chain genes from a single construct
648 upon transfection (Chng et al., 2015). For antibody production, we performed transfection of
649 ExpiCHO cell cultures using the Gibco ExpiCHO Expression System as described by the vendor.
650 IgG molecules were purified from culture supernatants using HiTrap MabSelect SuRe (Cytiva) on
651 a 24-column parallel protein chromatography system (Protein BioSolutions). Fab proteins were
652 purified using CaptureSelect column (Thermo Fisher Scientific). Purified antibodies were buffer-
653 exchanged into PBS, concentrated using Amicon Ultra-4 50-kDa (IgG) or 30 kDa (Fab) centrifugal
654 filter units (Millipore Sigma) and stored at 4°C until use. F(ab')₂ fragments were generated after
655 cleavage of IgG with IdeS protease (Promega) and then purified using TALON metal affinity resin
656 (Takara) to remove the enzyme and protein A agarose (Pierce) to remove the Fc fragment. Purified
657 mAbs were tested routinely for endotoxin levels (found to be less than 30 EU per mg IgG).
658 Endotoxin testing was performed using the PTS201F cartridge (Charles River), with a sensitivity
659 range from 10 to 0.1 EU per mL, and an Endosafe Nexgen-MCS instrument (Charles River).

660
661 **ELISA binding assays.** Wells of 96-well microtiter plates were coated with purified recombinant
662 SARS-CoV-2 S6P_{ecto}, SARS-CoV-2 S NTD, or SARS-CoV-2 RBS protein at 4 °C overnight.
663 Plates were blocked with 2% non-fat dry milk and 2% normal goat serum in Dulbecco's phosphate-
664 buffered saline (DPBS) containing 0.05% Tween-20 (DPBS-T) for 1 h. The bound antibodies were
665 detected using goat anti-human IgG conjugated with horseradish peroxidase (HRP) (Southern
666 Biotech, cat. 2040-05, lot B3919-XD29, 1:5,000 dilution) and a 3,3',5,5'-tetramethylbenzidine
667 (TMB) substrate (Thermo Fisher Scientific). Color development was monitored, 1M HCl was
668 added to stop the reaction, and the absorbance was measured at 450 nm using a spectrophotometer
669 (Biotek). For dose-response assays, serial dilutions of purified mAbs were applied to the wells in

670 triplicate, and antibody binding was detected as detailed above. EC₅₀ values for binding were
671 determined using Prism v.8.0 software (GraphPad) after log transformation of the mAb
672 concentration using sigmoidal dose–response nonlinear regression analysis.

673

674 **Focus reduction neutralization test (FRNT).** Serial dilutions of mAbs were incubated with
675 10² FFU of SARS-CoV-2 for 1 h at 37 °C. The antibody-virus complexes were added to Vero E6
676 cell-culture monolayers in 96-well plates for 1 h at 37 °C. Cells then were overlaid with 1% (w/v)
677 methylcellulose in minimum essential medium (MEM) supplemented to contain 2% heat-
678 inactivated FBS. Plates were fixed 30 h later by removing overlays and fixed with 4%
679 paraformaldehyde (PFA) in PBS for 20 min at room temperature. The plates were incubated
680 sequentially with 1 µg/mL of rCR3022 anti-S antibody or an murine anti-SARS-COV-2 mAb,
681 SARS2-16 (hybridoma supernatant diluted 1:6,000 to a final concentration of ~20 ng/mL) and
682 then HRP-conjugated goat anti-human IgG (Sigma-Aldrich, A6029) in PBS supplemented with
683 0.1% (w/v) saponin (Sigma) and 0.1% BSA. SARS-CoV-2-infected cell foci were visualized using
684 TrueBlue peroxidase substrate (KPL) and quantitated on an ImmunoSpot 5.0.37 Macro Analyzer
685 (Cellular Technologies). IC₅₀ values were determined by nonlinear regression analysis (with a
686 variable slope) using Prism software.

687

688 **Real-time cell analysis (RTCA) neutralization assay.** To determine neutralizing activity of IgG,
689 Fab, or F(ab')₂ proteins, we used real-time cell analysis (RTCA) assay on an xCELLigence RTCA
690 MP Analyzer (ACEA Biosciences Inc.) that measures virus-induced cytopathic effect (CPE)
691 (Gilchuk et al., 2020a; Zost et al., 2020b). Briefly, 50 µL of cell culture medium (DMEM
692 supplemented with 2% FBS) was added to each well of a 96-well E-plate using a ViaFlo384 liquid

693 handler (Integra Biosciences) to obtain background reading. A suspension of 18,000 Vero-E6 cells
694 in 50 μ L of cell culture medium was seeded in each well, and the plate was placed on the analyzer.
695 Measurements were taken automatically every 15 min, and the sensograms were visualized using
696 RTCA software version 2.1.0 (ACEA Biosciences Inc). VSV-SARS-CoV-2 (0.01 MOI, \sim 120 PFU
697 per well) was mixed 1:1 with a dilution of mAb in a total volume of 100 μ L using DMEM
698 supplemented with 2% FBS as a diluent and incubated for 1 h at 37°C in 5% CO₂. At 16 h after
699 seeding the cells, the virus-mAb mixtures were added in replicates to the cells in 96-well E-plates.
700 Triplicate wells containing virus only (maximal CPE in the absence of mAb) and wells containing
701 only Vero cells in medium (no-CPE wells) were included as controls. Plates were measured
702 continuously (every 15 min) for 48 h to assess virus neutralization. Normalized cellular index (CI)
703 values at the endpoint (48 h after incubation with the virus) were determined using the RTCA
704 software version 2.1.0 (ACEA Biosciences Inc.). Results are expressed as percent neutralization
705 in a presence of respective mAb relative to control wells with no CPE minus CI values from control
706 wells with maximum CPE. RTCA IC₅₀ values were determined by nonlinear regression analysis
707 using Prism software.

708

709 **Pre- and post-attachment neutralization assays.** For pre-attachment assays, serial dilutions of
710 mAbs were prepared at 4°C in Dulbecco's modified Eagle medium (DMEM) with 2% FBS and
711 preincubated with 10² FFU of SARS-CoV-2 for 1 h at 4°C. MAb-virus complexes were added to
712 a monolayer of Vero cells for 1 h at 4°C. Virus was allowed to internalize during a 37°C incubation
713 for 30 min. Cells were overlaid with 1% (wt/vol) methylcellulose in MEM. For post-attachment
714 assays, 2 x 10² FFU of SARS-CoV-2 was adsorbed onto a monolayer of Vero cells for 1 h at 4°C.
715 After removal of unbound virus, cells were washed twice with cold DMEM, followed by the

716 addition of serial dilutions of MAbs in cold DMEM. Virus-adsorbed cells were incubated with
717 mAd dilutions for 1 h at 4°C. Virus then was allowed to internalize for 30 min at 37°C, and
718 subsequently cells were overlaid with methylcellulose as described above. Thirty hours later, the
719 plates were fixed with 4% PFA and analyzed for antigen-specific foci as described above for
720 FRNTs.

721
722 **Attachment inhibition assay.** SARS-COV-2 was incubated with mAbs at the specified
723 concentration for 1 h at 4°C. The mixture was added to pre-chilled Vero or
724 Vero+ACE2+TMPRSS2 cells at an MOI of 0.005 and incubated at 4°C for 1 h. Cells were washed
725 six times with chilled PBS before addition of lysis buffer and extraction of RNA using MagMax
726 viral RNA isolation kit (Thermo Fisher Scientific) and a Kingfisher Flex 96-well extraction
727 machine (Thermo Fisher Scientific). SARS-CoV-2 RNA was quantified by qRT-PCR using the
728 N-specific primer/ probe set described below. Viral RNA levels were normalized to GAPDH, and
729 the fold change was compared with isotype control mAb.

730
731 **Human ACE2 binding inhibition analysis.** Wells of 384-well microtiter plates were coated
732 with 1 µg/mL purified recombinant SARS-CoV-2 S2P_{ecto} protein at 4°C overnight. Plates were
733 blocked with 2% non-fat dry milk and 2% normal goat serum in DPBS-T for 1 h. For screening
734 assays, purified mAbs from microscale expression were diluted two-fold in blocking buffer
735 starting from 10 µg/mL in triplicate, added to the wells (20 µL per well) and incubated for 1 h at
736 ambient temperature. Recombinant human ACE2 with a C-terminal Flag tag peptide was added to
737 wells at 2 µg/mL in a 5 µL per well volume (final 0.4 µg/mL concentration of human ACE2)
738 without washing of antibody and then incubated for 40 min at ambient temperature. Plates were

739 washed and bound human ACE2 was detected using HRP-conjugated anti-Flag antibody (Sigma-
740 Aldrich, cat. A8592, lot SLBV3799, 1:5,000 dilution) and TMB substrate. ACE2 binding without
741 antibody served as a control. The signal obtained for binding of the human ACE2 in the presence
742 of each dilution of tested antibody was expressed as a percentage of the human ACE2 binding
743 without antibody after subtracting the background signal. For dose–response assays, serial
744 dilutions of purified mAbs were applied to the wells in triplicate, and mAb binding was detected
745 as detailed above. IC₅₀ values for inhibition by mAb of S2P_{ecto} protein binding to human ACE2
746 was determined after log transformation of antibody concentration using sigmoidal dose–response
747 nonlinear regression analysis.

748

749 **Electron microscopy negative stain grid preparation, imaging and processing of S6P_{ecto}–Fab**

750 **complexes.** To perform electron microscopy imaging, Fabs were recombinantly expressed and
751 purified or produced by digesting recombinant chromatography-purified IgGs using resin-
752 immobilized cysteine protease enzyme (FabALACTICA, Genovis). The digestion occurred in 100
753 mM sodium phosphate and 150 mM NaCl pH 7.2 (PBS) for around 16 h at ambient temperature.
754 To remove cleaved Fc from intact IgG, the digestion mix was incubated with CaptureSelect Fc
755 resin (Genovis) for 30 min at ambient temperature in PBS buffer. If needed, the Fab was buffer-
756 exchanged into Tris buffer by centrifugation with a Zeba spin column (Thermo Fisher Scientific).

757

758 For screening and imaging of negatively-stained SARS-CoV-2 S6P_{ecto} protein in complex with
759 human Fabs, the proteins were incubated at an Fab:spike monomer molar ratio of 4:3 for about 1
760 hour at ambient temperature, and approximately 3 µL of the sample at concentrations of about 10–
761 15 µg/mL was applied to a glow-discharged grid with continuous carbon film on 400 square mesh

762 copper electron microscopy grids (Electron Microscopy Sciences). The grids were stained with
763 0.75% uranyl formate (Ohi et al., 2004) . Images were recorded on a Gatan US4000 4k × 4k CCD
764 camera using an FEI TF20 (TFS) transmission electron microscope operated at 200 keV and
765 control with Serial EM. All images were taken at 50,000× magnification with a pixel size of 2.18
766 Å per pixel in low-dose mode at a defocus of 1.5 to 1.8 µm. The total dose for the micrographs
767 was around 30e⁻ per Å². Image processing was performed using the cryoSPARC software
768 package. Images were imported, CTF-estimated and particles were picked. The particles were
769 extracted with a box size of 256 pixels and binned to 128 pixels. 2D class averages were performed
770 and good classes selected for *ab initio* model and refinement without symmetry. Model docking
771 to the EM map was done in Chimera (Pettersen et al., 2004). For SARS-CoV-2 S6P_{ecto} protein, the
772 closed model (PDB:7JJI) was used and PDB:12E8 was used for the Fab (see also **Table S2** for
773 details).

774
775 **Epitope mapping of antibodies by alanine-scanning mutagenesis.** Epitope mapping was
776 performed essentially as described previously (Davidson and Doranz, 2014) using a SARS-CoV-
777 2 (strain Wuhan-Hu-1) spike protein NTD shotgun mutagenesis mutation library, made using a
778 full-length expression construct for spike protein, where 215 residues of the NTD (between spike
779 residues 9 and 310) were mutated individually to alanine, and alanine residues to serine. Mutations
780 were confirmed by DNA sequencing, and clones arrayed in a 384-well plate, one mutant per well.
781 Binding of mAbs to each mutant clone in the alanine scanning library was determined, in duplicate,
782 by high-throughput flow cytometry. A plasmid encoding cDNA for each spike protein mutant was
783 transfected into HEK-293T cells and allowed to express for 22 h. Cells were fixed in 4% (v/v)
784 paraformaldehyde (Electron Microscopy Sciences), and permeabilized with 0.1% (w/v) saponin

785 (Sigma-Aldrich) in PBS plus calcium and magnesium (PBS++) before incubation with mAbs
786 diluted in PBS++, 10% normal goat serum (Sigma), and 0.1% saponin. MAb screening
787 concentrations were determined using an independent immunofluorescence titration curve against
788 cells expressing wild-type S protein to ensure that signals were within the linear range of detection.
789 Antibodies were detected using 3.75 µg/mL of Alexa-Fluor-488-conjugated secondary antibodies
790 (Jackson ImmunoResearch Laboratories) in 10% normal goat serum with 0.1% saponin. Cells
791 were washed three times with PBS++/0.1% saponin followed by two washes in PBS, and mean
792 cellular fluorescence was detected using a high-throughput Intellicyte iQue flow cytometer
793 (Sartorius). Antibody reactivity against each mutant S protein clone was calculated relative to
794 wild-type S protein reactivity by subtracting the signal from mock-transfected controls and
795 normalizing to the signal from wild-type S-transfected controls. Mutations within clones were
796 identified as critical to the mAb epitope if they did not support reactivity of the test MAb, but
797 supported reactivity of other SARS-CoV-2 antibodies. This counter-screen strategy facilitates the
798 exclusion of S protein mutants that are locally misfolded or have an expression defect.

799

800 **Selection of virus escape mutants using the S protein-expressing VSV.** To screen for escape
801 mutations selected in the presence of individual mAbs, we used a modification of the RTCA assay
802 as recently described (Greaney et al., 2021). Fifty µL of cell culture medium (DMEM
803 supplemented with 2% FBS) was added to each well of a 96-well E-plate to obtain a background
804 reading. A suspension of 18,000 Vero E6 cells in 50 µL of cell culture medium was seeded per
805 each well, and plates were placed on the analyzer. Measurements were taken automatically every
806 15 min and the sensograms were visualized using RTCA software version 2.1.0 (ACEA
807 Biosciences Inc). VSV-SARS-CoV-2 virus (5,000 PFU per well, ~0.3 MOI) was mixed with a

808 saturating neutralizing concentration of COV2-2676 (5 µg/mL) and COV2-2489 (50 µg/mL) in a
809 total volume of 100 mL and incubated for 1 h at 37°C. At 16 to 20 h after seeding the cells, the
810 virus-antibody mixtures were added into 1 to 88 replicate wells of 96-well E-plates with cell
811 monolayers. Wells containing only virus in the absence of antibody and wells containing only
812 Vero E6 cells in medium were included on each plate as controls. Plates were measured
813 continuously (every 15 min) for 72 h. The escape mutants were identified by unexpectedly high
814 CPE in wells containing neutralizing antibody. To verify escape from antibody selection, isolated
815 viruses were assessed in a subsequent RTCA experiment in the presence of 10 µg/mL (COV2-
816 2676) and 100 µg/mL (COV2-2489) of mAb as used for the escape virus selection.

817

818 **Sequence analysis of the gene encoding S protein from S protein-expressing VSV escape**
819 **mutants.** To identify escape mutations present in S protein-expressing VSV mAb-selected escape
820 variants, the escape viruses isolated after RTCA escape screening were propagated in 6-well
821 culture plates with confluent Vero E6 cells in the presence of 10 µg/mL of the corresponding
822 antibody. Viral RNA was isolated using a QiAmp Viral RNA extraction kit (QIAGEN) from
823 aliquots of supernatant containing a suspension of the selected virus population. The S protein
824 gene cDNA was amplified with a SuperScript IV One-Step RT-PCR kit (Thermo Fisher Scientific)
825 using primers flanking the S gene. The amplified PCR product (4,000 bp) was purified using SPRI
826 magnetic beads (Beckman Coulter) at a 1:1 ratio and sequenced by the Sanger sequence technique
827 using primers giving forward and reverse reads of the NTD.

828

829 **MAB binding to the surface of SARS-CoV-2 infected cells.** Vero E6 cells were inoculated with
830 SARS-CoV-2 at an MOI of 0.01. At 48 h post-infection, cells were trypsinized and resuspended

831 in a staining buffer composed of DPBS with 5% FBS, 5 mM EDTA, 0.05% NaN₃. mAbs were
832 diluted in the staining buffer and incubated with ~3 x 10⁴ cells for 30 min at 4°C. Cells were
833 washed twice and incubated with Alexa Fluor 647-conjugated secondary antibody (Invitrogen)
834 diluted 1:1,000 in staining buffer for 30 min at 4°C. Cells were washed twice and fixed with 4%
835 PFA prior to detection of fluorescence signal by flow cytometry (MacQuant) and analysis using
836 FlowJo software.

837
838 **Protection against wild-type SARS-CoV-2 in mice.** Male and female heterozygous K18-hACE
839 C57BL/6J mice were housed in groups of up to 5 mice per cage at 18 to 24°C ambient temperatures
840 and 40 to 60% humidity. Mice were fed a 20% protein diet (PicoLab 5053, Purina) and maintained on
841 a 12-h light–dark cycle (06:00 to 18:00). Food and water were available *ad libitum*. Mice (8 to 9 weeks
842 old) were inoculated with 1 × 10³ PFU of SARS-CoV-2 via the intranasal route. Anti-SARS-CoV-2
843 human mAbs or isotype control mABS were administered 24 h before (prophylaxis) or 24 h or 48 h
844 after (therapy) SARS-CoV-2 inoculation. Weights and lethality were monitored on a daily basis for
845 up to 14 days after inoculation and a subset of mice were euthanized at 7 dpi and tissues were collected.

846
847 **Measurement of viral burden.** For RT–qPCR, mouse tissues were weighed and homogenized
848 with zirconia beads in a MagNA Lyser instrument (Roche Life Science) in 1 mL of DMEM
849 medium supplemented with 2% heat-inactivated FBS. Tissue homogenates were clarified by
850 centrifugation at 10,000 rpm for 5 min and stored at –80°C. RNA was extracted using a MagMax
851 mirVana Total RNA isolation kit (Thermo Fisher Scientific) and a Kingfisher Flex 96-well
852 extraction machine (Thermo Fisher Scientific). RNA was reverse transcribed and amplified using
853 the TaqMan RNA-to-CT 1-Step Kit (ThermoFisher). RNA levels were measured by one-step

854 quantitative reverse transcriptase PCR (qRT-PCR) assay as previously described (Hassan *et al.*,
855 2020). A TaqMan assay was designed to target the N gene, as previously described (Case; PMID
856 32838945). Specific primers and probe were used: Forward primer:
857 ATGCTGCAATCGTGCTACAA; Reverse primer: GACTGCCGCCTCTGCTC; Probe: /56-
858 FAM/TCAAGGAAC/ZEN/AACATTGCCAA/3IABkFQ/. N gene copy numbers were
859 determined down to 10 copies per reaction.

860

861 **ELISA to detect recombinant human mAbs**

862 Goat anti-human kappa cross-absorbed against mouse IgG (Southern Biotech catalog # 2061-01) and
863 goat anti-human lambda cross-absorbed against mouse IgG (Southern Biotech catalog # 2071-01)
864 were coated onto 96-well Nunc Maxisorp flat-bottomed plates at 2 µg/mL in coating buffer (0.1 M
865 sodium carbonate, 0.1 M sodium bicarbonate, 0.02% NaN₃, pH 9.6) overnight at 4°C. Coating buffers
866 were aspirated, and wells were blocked with 2% BSA (blocking buffer) (Fisher Bioreagents catalog #
867 BP1600-100), for 1 h at 37°C. Heat-inactivated serum samples were diluted in blocking buffer in a
868 separate polypropylene plate. The plates then were washed 4× with 1× PBS + 0.05% Tween-20
869 (PBST) (Fisher Bioreagents catalog # BP337-100), followed by addition of 50 µL of respective serum
870 dilutions and was incubated for 1 h at 4°C. The ELISA plates were again washed 4× in PBST, followed
871 by addition of 50 µL of 1:2,000 Goat Anti-Human IgG Fc, Multi-Species (Southern Biotech catalog
872 # 2014-05). Plates were incubated for 1 h at 4°C. Plates were washed with 4× PBST, followed by 100
873 µL of TMB-ELISA substrate (Thermo Fisher Scientific catalog # 34028) and incubated at room
874 temperature for 3 to 5 min. Color development was observed and reactions were stopped with 50 µL
875 of 2N sulfuric acid. Optical density (450 nm) measurements were determined using a microplate reader
876 (Bio-Rad).

877
878 **Cytokine and chemokine protein measurements.** Lung homogenates were incubated with Triton-
879 X-100 (1% final concentration) for 1 h at room temperature to inactivate SARS-CoV-2. The samples
880 were then analyzed by Eve Technologies Corporation (Calgary, AB, Canada). Cytokine and
881 chemokine protein expression were determined using the Mouse Cytokine Array / Chemokine Array
882 31-Plex (MD31) platform. Fold-change was calculated by comparing anti-SARS-CoV-2-specific or
883 isotype-control mAb-treated mice to naive control mice.

884
885 **Lung histology.** Mice were euthanized and tissues were harvested before lung was inflation and
886 fixation. The left lung was first tied off at the left main bronchus and collected for viral RNA analysis.
887 The right lung was inflated with approximately with 1.2 mL of 10% neutral buffered formalin using a
888 3-mL syringe and catheter inserted into the trachea. The inflated lung was then kept in 40 mL neutral
889 buffered formalin for 7 days. Tissues were embedded in paraffin, and sections were stained with
890 hematoxylin and eosin. Tissue sections were then scanned using Hamamatsu NanoZoomer slide
891 scanning system. Scanned image was then viewed by using the NDP view software (ver.1.2.46).

892
893 **QUANTIFICATION AND STATISTICAL ANALYSIS**
894 Mean \pm S.E.M. or mean \pm S.D. were determined for continuous variables as noted. Technical and
895 biological replicates are described in the figure legends. For analysis of mouse studies, the
896 comparison of weight-change curves was performed using a one-way ANOVA with Dunnett's
897 post hoc test using Prism v.9.0 (GraphPad). Viral burden and gene-expression measurements were
898 compared to each other or the isotype control using a one-way ANOVA with Tukey's or Dunnett's
899 post hoc test, respectively, using Prism v.9.0 (GraphPad). Survival curves were estimated using

900 the Kaplan-Meier method and differences assessed using the log-rank Mantel-Cox test and a
901 Bonferroni correction for multiple comparisons using Prism v.9.0 (GraphPad).

902 **REFERENCES**

903
904 Alsoussi, W.B., Turner, J.S., Case, J.B., Zhao, H., Schmitz, A.J., Zhou, J.Q., Chen, R.E., Lei, T.,
905 Rizk, A.A., McIntire, K.M., et al. (2020). A potentially neutralizing antibody protects mice against
906 SARS-CoV-2 infection. *J Immunol* 205, 915-922.

907
908 Atyeo, C., Fischinger, S., Zohar, T., Slein, M.D., Burke, J., Loos, C., McCulloch, D.J., Newman,
909 K.L., Wolf, C., Yu, J., et al. (2020). Distinct early serological signatures track with SARS-CoV-2
910 survival. *Immunity* 53, 524-532 e524.

911
912 Avanzato, V.A., Matson, M.J., Seifert, S.N., Pryce, R., Williamson, B.N., Anzick, S.L., Barbian,
913 K., Judson, S.D., Fischer, E.R., Martens, C., et al. (2020). Case Study: Prolonged infectious
914 SARS-CoV-2 shedding from an asymptomatic immunocompromised individual with cancer.
915 *Cell* 183, 1901-1912 e1909.

916
917 Barnes, C.O., West, A.P., Jr., Huey-Tubman, K.E., Hoffmann, M.A.G., Sharaf, N.G., Hoffman,
918 P.R., Koranda, N., Gristick, H.B., Gaebler, C., Muecksch, F., et al. (2020). Structures of human
919 antibodies bound to SARS-CoV-2 spike reveal common epitopes and recurrent features of
920 antibodies. *Cell* 182, 828-842 e816.

921
922 Baum, A., Ajithdoss, D., Copin, R., Zhou, A., Lanza, K., Negron, N., Ni, M., Wei, Y.,
923 Mohammadi, K., Musser, B., et al. (2020a). REGN-COV2 antibodies prevent and treat SARS-
924 CoV-2 infection in rhesus macaques and hamsters. *Science* 370, 1110-1115.

925

926 Baum, A., Fulton, B.O., Wloga, E., Copin, R., Pascal, K.E., Russo, V., Giordano, S., Lanza, K.,
927 Negron, N., Ni, M., et al. (2020b). Antibody cocktail to SARS-CoV-2 spike protein prevents
928 rapid mutational escape seen with individual antibodies. *Science* 369, 1014-1018.

929

930 Bloch, E.M. (2020). Convalescent plasma to treat COVID-19. *Blood* 136, 654-655.

931

932 Brouwer, P.J.M., Caniels, T.G., van der Straten, K., Snitselaar, J.L., Aldon, Y., Bangaru, S.,
933 Torres, J.L., Okba, N.M.A., Claireaux, M., Kerster, G., et al. (2020). Potent neutralizing
934 antibodies from COVID-19 patients define multiple targets of vulnerability. *Science* 369, 643-
935 650.

936

937 Cantuti-Castelvetri, L., Ojha, R., Pedro, L.D., Djannatian, M., Franz, J., Kuivanen, S., van der
938 Meer, F., Kallio, K., Kaya, T., Anastasina, M., et al. (2020). Neuropilin-1 facilitates SARS-CoV-
939 2 cell entry and infectivity. *Science* 370, 856-860.

940

941 Cao, Y., Su, B., Guo, X., Sun, W., Deng, Y., Bao, L., Zhu, Q., Zhang, X., Zheng, Y., Geng, C.,
942 et al. (2020). Potent neutralizing antibodies against SARS-CoV-2 identified by high-throughput
943 single-cell sequencing of convalescent patients' B cells. *Cell* 182, 73-84 e16.

944

945 Case, J.B., Bailey, A.L., Kim, A.S., Chen, R.E., and Diamond, M.S. (2020a). Growth, detection,
946 quantification, and inactivation of SARS-CoV-2. *Virology* 548, 39-48.

947

948 Case, J.B., Rothlauf, P.W., Chen, R.E., Liu, Z., Zhao, H., Kim, A.S., Bloyet, L.M., Zeng, Q.,
949 Tahan, S., Droit, L., et al. (2020b). Neutralizing antibody and soluble ACE2 inhibition of a
950 replication-competent VSV-SARS-CoV-2 and a clinical isolate of SARS-CoV-2. *Cell Host*
951 *Microbe* 28, 475-485 e475.

952

953 Chen, P., Nirula, A., Heller, B., Gottlieb, R.L., Boscia, J., Morris, J., Huhn, G., Cardona, J.,
954 Mocherla, B., Stosor, V., et al. (2020a). SARS-CoV-2 neutralizing antibody LY-CoV555 in
955 outpatients with Covid-19. *N Engl J Med* 101056/NEJMoa2029849.

956

957 Chen, P.F., Yu, X.X., Liu, Y.P., Ren, D., Shen, M., Huang, B.S., Gao, J.L., Huang, Z.Y., Wu,
958 M., Wang, W.Y., et al. (2020b). Virus load and virus shedding of SARS-CoV-2 and their impact
959 on patient outcomes. *World J Clin Cases* 8, 6252-6263.

960

961 Chi, X., Yan, R., Zhang, J., Zhang, G., Zhang, Y., Hao, M., Zhang, Z., Fan, P., Dong, Y., Yang,
962 Y., et al. (2020). A neutralizing human antibody binds to the N-terminal domain of the Spike
963 protein of SARS-CoV-2. *Science* 369, 650-655.

964

965 Chiodo, F., Bruijns, S.C.M., Rodriguez, E., Li, R.J.E., Molinaro, A., Silipo, A., Di Lorenzo, F.,
966 Garcia-Rivera, D., Valdes-Balbin, Y., Verez-Bencomo, V., et al. (2020). Novel ACE2-
967 independent carbohydrate-binding of SARS-CoV-2 spike protein to host lectins and lung
968 microbiota. *bioRxiv*, 2020.2005.2013.092478.

969

970 Chng, J., Wang, T., Nian, R., Lau, A., Hoi, K.M., Ho, S.C., Gagnon, P., Bi, X., and Yang, Y.
971 (2015). Cleavage efficient 2A peptides for high level monoclonal antibody expression in CHO
972 cells. *MAbs* 7, 403-412.
973
974 Choi, B., Choudhary, M.C., Regan, J., Sparks, J.A., Padera, R.F., Qiu, X., Solomon, I.H., Kuo,
975 H.H., Boucau, J., Bowman, K., et al. (2020). Persistence and evolution of SARS-CoV-2 in an
976 immunocompromised Host. *N Engl J Med* 383, 2291-2293.
977
978 Clausen, T.M., Sandoval, D.R., Spliid, C.B., Pihl, J., Perrett, H.R., Painter, C.D., Narayanan, A.,
979 Majowicz, S.A., Kwong, E.M., McVicar, R.N., et al. (2020). SARS-CoV-2 infection depends on
980 cellular heparan sulfate and ACE2. *Cell* 183, 1043-1057 e1015.
981
982 Davidson, E., and Doranz, B.J. (2014). A high-throughput shotgun mutagenesis approach to
983 mapping B-cell antibody epitopes. *Immunology* 143, 13-20.
984
985 DiLillo, D.J., Tan, G.S., Palese, P., and Ravetch, J.V. (2014). Broadly neutralizing
986 hemagglutinin stalk-specific antibodies require FcγR interactions for protection against
987 influenza virus in vivo. *Nat Med* 20, 143-151.
988
989 Fox, J.M., Roy, V., Gunn, B.M., Huang, L., Edeling, M.A., Mack, M., Fremont, D.H., Doranz,
990 B.J., Johnson, S., Alter, G., et al. (2019). Optimal therapeutic activity of monoclonal antibodies
991 against chikungunya virus requires Fc-FcγR interaction on monocytes. *Sci Immunol* 4
992 eaav5062.

993 Gao, S., and Zhang, L. (2020). ACE2 partially dictates the host range and tropism of SARS-
994 CoV-2. *Comput Struct Biotechnol J* 18, 4040-4047.
995
996 Gilchuk, P., Bombardi, R.G., Erasmus, J.H., Tan, Q., Nargi, R., Soto, C., Abbink, P., Suscovich,
997 T.J., Durnell, L.A., Khandhar, A., et al. (2020a). Integrated pipeline for the accelerated discovery
998 of antiviral antibody therapeutics. *Nat Biomed Eng* 4, 1030-1043.
999
1000 Gilchuk, P., Murin, C.D., Milligan, J.C., Cross, R.W., Mire, C.E., Ilinykh, P.A., Huang, K.,
1001 Kuzmina, N., Altman, P.X., Hui, S., et al. (2020b). Analysis of a therapeutic antibody cocktail
1002 reveals determinants for cooperative and broad ebolavirus neutralization. *Immunity* 52, 388-403
1003 e312.
1004
1005 Golden, J.W., Cline, C.R., Zeng, X., Garrison, A.R., Carey, B.D., Mucker, E.M., White, L.E.,
1006 Shamblin, J.D., Brocato, R.L., Liu, J., et al. (2020). Human angiotensin-converting enzyme 2
1007 transgenic mice infected with SARS-CoV-2 develop severe and fatal respiratory disease. *JCI*
1008 *Insight* 5(19):e142032.
1009
1010 Greaney, A.J., Starr, T.N., Gilchuk, P., Zost, S.J., Binshtein, E., Loes, A.N., Hilton, S.K.,
1011 Huddleston, J., Eguia, R., Crawford, K.H.D., et al. (2021). Complete mapping of mutations to
1012 the SARS-CoV-2 spike receptor-binding domain that escape antibody recognition. *Cell Host*
1013 *Microbe* 29, 44-57 e49.
1014

1015 Halper-Stromberg, A., Lu, C.L., Klein, F., Horwitz, J.A., Bournazos, S., Nogueira, L.,
1016 Eisenreich, T.R., Liu, C., Gazumyan, A., Schaefer, U., et al. (2014). Broadly neutralizing
1017 antibodies and viral inducers decrease rebound from HIV-1 latent reservoirs in humanized mice.
1018 *Cell* 158, 989-999.

1019

1020 Hansen, J., Baum, A., Pascal, K.E., Russo, V., Giordano, S., Wloga, E., Fulton, B.O., Yan, Y.,
1021 Koon, K., Patel, K., et al. (2020). Studies in humanized mice and convalescent humans yield a
1022 SARS-CoV-2 antibody cocktail. *Science* 369, 1010-1014.

1023

1024 Harcourt, J., Tamin, A., Lu, X., Kamili, S., Sakthivel, S.K., Murray, J., Queen, K., Tao, Y.,
1025 Paden, C.R., Zhang, J., et al. (2020a). Isolation and characterization of SARS-CoV-2 from the
1026 first US COVID-19 patient. *bioRxiv* 101101/20200302972935, 2020.2003.2002.972935.

1027

1028 Harcourt, J., Tamin, A., Lu, X., Kamili, S., Sakthivel, S.K., Murray, J., Queen, K., Tao, Y.,
1029 Paden, C.R., Zhang, J., et al. (2020b). Severe acute respiratory syndrome coronavirus 2 from
1030 patient with coronavirus disease, United States. *Emerg Infect Dis* 26, 1266-1273.

1031

1032 Hassan, A.O., Case, J.B., Winkler, E.S., Thackray, L.B., Kafai, N.M., Bailey, A.L., McCune,
1033 B.T., Fox, J.M., Chen, R.E., Alsoussi, W.B., et al. (2020). A SARS-CoV-2 infection model in
1034 mice demonstrates protection by neutralizing antibodies. *Cell* 182, 744-753 e744.

1035

- 1036 Hou, Y.J., Chiba, S., Halfmann, P., Ehre, C., Kuroda, M., Dinnon, K.H., 3rd, Leist, S.R.,
1037 Schafer, A., Nakajima, N., Takahashi, K., et al. (2020). SARS-CoV-2 D614G variant exhibits
1038 efficient replication ex vivo and transmission in vivo. *Science* 370, 1464-1468.
1039
1040 Hsieh, C.L., Goldsmith, J.A., Schaub, J.M., DiVenere, A.M., Kuo, H.C., Javanmardi, K., Le,
1041 K.C., Wrapp, D., Lee, A.G., Liu, Y., et al. (2020). Structure-based design of prefusion-stabilized
1042 SARS-CoV-2 spikes. *Science* 369, 1501-1505.
1043
1044 Jones, B.E., Brown-Augsburger, P.L., Corbett, K.S., Westendorf, K., Davies, J., Cujec, T.P.,
1045 Wiethoff, C.M., Blackbourne, J.L., Heinz, B.A., Foster, D., et al. (2020). LY-CoV555, a rapidly
1046 isolated potent neutralizing antibody, provides protection in a non-human primate model of
1047 SARS-CoV-2 infection. *bioRxiv* 101101/20200930318972.
1048
1049 Ju, B., Zhang, Q., Ge, J., Wang, R., Sun, J., Ge, X., Yu, J., Shan, S., Zhou, B., Song, S., et al.
1050 (2020). Human neutralizing antibodies elicited by SARS-CoV-2 infection. *Nature* 584, 115-119.
1051
1052 Kemp, S., Harvey, W., Datir, R., Collier, D., Ferreira, I., Carabelli, A., Robertson, D., and Gupta,
1053 R. (2020). Recurrent emergence and transmission of a SARS-CoV-2 Spike deletion Δ H69/V70.
1054 *bioRxiv* 20201214422555, 2020.2012.2014.422555.
1055
1056 Laczko, D., Hogan, M.J., Toulmin, S.A., Hicks, P., Lederer, K., Gaudette, B.T., Castano, D.,
1057 Amanat, F., Muramatsu, H., Oguin, T.H., 3rd, et al. (2020). A single immunization with

1058 nucleoside-modified mRNA vaccines elicits strong cellular and humoral immune responses
1059 against SARS-CoV-2 in mice. *Immunity* 53, 724-732 e727.
1060
1061 Liu, L., Wang, P., Nair, M.S., Yu, J., Rapp, M., Wang, Q., Luo, Y., Chan, J.F., Sahi, V.,
1062 Figueroa, A., et al. (2020a). Potent neutralizing antibodies against multiple epitopes on SARS-
1063 CoV-2 spike. *Nature* 584, 450-456.
1064
1065 Liu, Z., Zheng, H., Lin, H., Li, M., Yuan, R., Peng, J., Xiong, Q., Sun, J., Li, B., Wu, J., et al.
1066 (2020b). Identification of common deletions in the spike protein of severe acute respiratory
1067 syndrome coronavirus 2. *J Virol* 94 e00790-20.
1068
1069 Lu, C.L., Murakowski, D.K., Bournazos, S., Schoofs, T., Sarkar, D., Halper-Stromberg, A.,
1070 Horwitz, J.A., Nogueira, L., Golijanin, J., Gazumyan, A., et al. (2016). Enhanced clearance of
1071 HIV-1-infected cells by broadly neutralizing antibodies against HIV-1 in vivo. *Science* 352,
1072 1001-1004.
1073
1074 Lund, J., Winter, G., Jones, P.T., Pound, J.D., Tanaka, T., Walker, M.R., Artymiuk, P.J., Arata,
1075 Y., Burton, D.R., Jefferis, R., et al. (1991). Human Fc gamma RI and Fc gamma RII interact with
1076 distinct but overlapping sites on human IgG. *J Immunol* 147, 2657-2662.
1077
1078 McCallum, M., Marco, A.D., Lempp, F., Tortorici, M.A., Pinto, D., Walls, A.C., Beltramello,
1079 M., Chen, A., Liu, Z., Zatta, F., et al. (2021). N-terminal domain antigenic mapping reveals a site
1080 of vulnerability for SARS-CoV-2. *bioRxiv*, 2021.2001.2014.426475.

1081

1082 McCarthy, K.R., Rennick, L.J., Nambulli, S., Robinson-McCarthy, L.R., Bain, W.G., Haidar, G.,
1083 and Duprex, W.P. (2020). Natural deletions in the SARS-CoV-2 spike glycoprotein drive
1084 antibody escape. *bioRxiv* 2020.2011.2019.389916.

1085

1086 Mukherjee, S., Sirohi, D., Dowd, K.A., Chen, Z., Diamond, M.S., Kuhn, R.J., and Pierson, T.C.
1087 (2016). Enhancing dengue virus maturation using a stable furin over-expressing cell line.
1088 *Virology* 497, 33-40.

1089

1090 Mulligan, M.J., Lyke, K.E., Kitchin, N., Absalon, J., Gurtman, A., Lockhart, S., Neuzil, K.,
1091 Raabe, V., Bailey, R., Swanson, K.A., et al. (2020). Phase I/II study of COVID-19 RNA vaccine
1092 BNT162b1 in adults. *Nature* 586, 589-593.

1093

1094 Ohi, M., Li, Y., Cheng, Y., and Walz, T. (2004). Negative Staining and Image Classification -
1095 Powerful Tools in Modern Electron Microscopy. *Biol Proced Online* 6, 23-34.

1096

1097 Oladunni, F.S., Park, J.G., Pino, P.A., Gonzalez, O., Akhter, A., Allue-Guardia, A., Olmo-
1098 Fontanez, A., Gautam, S., Garcia-Vilanova, A., Ye, C., et al. (2020). Lethality of SARS-CoV-2
1099 infection in K18 human angiotensin-converting enzyme 2 transgenic mice. *Nat Commun* 11,
1100 6122.

1101

1102 Oude Munnink, B.B., Sikkema, R.S., Nieuwenhuijse, D.F., Molenaar, R.J., Munger, E.,
1103 Molenkamp, R., van der Spek, A., Tolsma, P., Rietveld, A., Brouwer, M., et al. (2021).

- 1104 Transmission of SARS-CoV-2 on mink farms between humans and mink and back to humans.
1105 Science 371, 172-177.
1106
- 1107 Pettersen, E.F., Goddard, T.D., Huang, C.C., Couch, G.S., Greenblatt, D.M., Meng, E.C., and
1108 Ferrin, T.E. (2004). UCSF Chimera--a visualization system for exploratory research and
1109 analysis. J Comput Chem 25, 1605-1612.
1110
- 1111 Piccoli, L., Park, Y.J., Tortorici, M.A., Czudnochowski, N., Walls, A.C., Beltramello, M.,
1112 Silacci-Fregni, C., Pinto, D., Rosen, L.E., Bowen, J.E., et al. (2020). Mapping neutralizing and
1113 immunodominant sites on the SARS-CoV-2 spike receptor-binding domain by structure-guided
1114 high-resolution serology. Cell 183, 1024-1042 e1021.
1115
- 1116 Pinto, D., Park, Y.J., Beltramello, M., Walls, A.C., Tortorici, M.A., Bianchi, S., Jaconi, S.,
1117 Culap, K., Zatta, F., De Marco, A., et al. (2020). Cross-neutralization of SARS-CoV-2 by a
1118 human monoclonal SARS-CoV antibody. Nature 583, 290-295.
1119
- 1120 Plante, J.A., Liu, Y., Liu, J., Xia, H., Johnson, B.A., Lokugamage, K.G., Zhang, X., Muruato,
1121 A.E., Zou, J., Fontes-Garfias, C.R., et al. (2020). Spike mutation D614G alters SARS-CoV-2
1122 fitness. Nature 101038/s41586-020-2895-3.
1123
- 1124 Rambaut, A., Holmes, E.C., O'Toole, A., Hill, V., McCrone, J.T., Ruis, C., du Plessis, L., and
1125 Pybus, O.G. (2020). A dynamic nomenclature proposal for SARS-CoV-2 lineages to assist
1126 genomic epidemiology. Nat Microbiol 5, 1403-1407.

1127

1128 Robbiani, D.F., Gaebler, C., Muecksch, F., Lorenzi, J.C.C., Wang, Z., Cho, A., Agudelo, M.,
1129 Barnes, C.O., Gazumyan, A., Finkin, S., et al. (2020). Convergent antibody responses to SARS-
1130 CoV-2 in convalescent individuals. *Nature* 584, 437-442.

1131

1132 Rogers, T.F., Zhao, F., Huang, D., Beutler, N., Burns, A., He, W.T., Limbo, O., Smith, C., Song,
1133 G., Woehl, J., et al. (2020). Isolation of potent SARS-CoV-2 neutralizing antibodies and
1134 protection from disease in a small animal model. *Science* 369, 956-963.

1135

1136 Schafer, A., Muecksch, F., Lorenzi, J.C.C., Leist, S.R., Cipolla, M., Bournazos, S., Schmidt, F.,
1137 Maison, R.M., Gazumyan, A., Martinez, D.R., et al. (2021). Antibody potency, effector function,
1138 and combinations in protection and therapy for SARS-CoV-2 infection in vivo. *J Exp Med* 218
1139 e20201993.

1140

1141 Seydoux, E., Homad, L.J., MacCamy, A.J., Parks, K.R., Hurlburt, N.K., Jennewein, M.F., Akins,
1142 N.R., Stuart, A.B., Wan, Y.H., Feng, J., et al. (2020). Analysis of a SARS-CoV-2-infected
1143 individual reveals development of potent neutralizing antibodies with limited somatic mutation.
1144 *Immunity* 53, 98-105 e105.

1145

1146 Smith, C.C., Entwistle, S., Willis, C., Vensko, S., Beck, W., Garness, J., Sambade, M., Routh, E.,
1147 Olsen, K., Kodysh, J., et al. (2020). Landscape and selection of vaccine epitopes in SARS-CoV-
1148 2. bioRxiv 101101/20200604135004.

1149

1150 Starr, T.N., Greaney, A.J., Addetia, A., Hannon, W.W., Choudhary, M.C., Dingens, A.S., Li,
1151 J.Z., and Bloom, J.D. (2020). Prospective mapping of viral mutations that escape antibodies used
1152 to treat COVID-19. *bioRxiv*, 2020.2011.2030.405472.
1153

1154 Tegally, H., Wilkinson, E., Giovanetti, M., Iranzadeh, A., Fonseca, V., Giandhari, J., Doolabh,
1155 D., Pillay, S., San, E.J., Msomi, N., et al. (2020). Emergence and rapid spread of a new severe
1156 acute respiratory syndrome-related coronavirus 2 (SARS-CoV-2) lineage with multiple spike
1157 mutations in South Africa. *medRxiv*, 2020.2012.2021.20248640.
1158

1159 ter Meulen, J., van den Brink, E.N., Poon, L.L., Marissen, W.E., Leung, C.S., Cox, F., Cheung,
1160 C.Y., Bakker, A.Q., Bogaards, J.A., van Deventer, E., et al. (2006). Human monoclonal antibody
1161 combination against SARS coronavirus: synergy and coverage of escape mutants. *PLoS Med* 3,
1162 e237.
1163

1164 Voss, W.N., Hou, Y.J., Johnson, N.V., Kim, J.E., Delidakis, G., Horton, A.P., Bartzoka, F.,
1165 Paresi, C.J., Tanno, Y., Abbasi, S.A., et al. (2020). Prevalent, protective, and convergent IgG
1166 recognition of SARS-CoV-2 non-RBD spike epitopes in COVID-19 convalescent plasma.
1167 *bioRxiv*, 2020.2012.2020.423708.
1168

1169 Wang, C., Li, W., Drabek, D., Okba, N.M.A., van Haperen, R., Osterhaus, A., van Kuppeveld,
1170 F.J.M., Haagmans, B.L., Grosveld, F., and Bosch, B.J. (2020). A human monoclonal antibody
1171 blocking SARS-CoV-2 infection. *Nat Commun* 11, 2251.
1172

1173 Wec, A.Z., Wrapp, D., Herbert, A.S., Maurer, D.P., Haslwanter, D., Sakharkar, M., Jangra, R.K.,
1174 Dieterle, M.E., Lilov, A., Huang, D., et al. (2020). Broad neutralization of SARS-related viruses
1175 by human monoclonal antibodies. *Science* 369, 731-736.
1176
1177 Weisblum, Y., Schmidt, F., Zhang, F., DaSilva, J., Poston, D., Lorenzi, J.C., Muecksch, F.,
1178 Rutkowska, M., Hoffmann, H.H., Michailidis, E., et al. (2020). Escape from neutralizing
1179 antibodies by SARS-CoV-2 spike protein variants. *Elife* 9 e61312.
1180
1181 Wines, B.D., Powell, M.S., Parren, P.W., Barnes, N., and Hogarth, P.M. (2000). The IgG Fc
1182 contains distinct Fc receptor (FcR) binding sites: the leukocyte receptors Fc gamma RI and Fc
1183 gamma RIIa bind to a region in the Fc distinct from that recognized by neonatal FcR and protein
1184 A. *J Immunol* 164, 5313-5318.
1185
1186 Winkler, E.S., Bailey, A.L., Kafai, N.M., Nair, S., McCune, B.T., Yu, J., Fox, J.M., Chen, R.E.,
1187 Earnest, J.T., Keeler, S.P., et al. (2020). SARS-CoV-2 infection of human ACE2-transgenic mice
1188 causes severe lung inflammation and impaired function. *Nat Immunol* 21, 1327-1335.
1189
1190 Wrapp, D., Wang, N., Corbett, K.S., Goldsmith, J.A., Hsieh, C.L., Abiona, O., Graham, B.S.,
1191 and McLellan, J.S. (2020). Cryo-EM structure of the 2019-nCoV spike in the prefusion
1192 conformation. *Science* 367, 1260-1263.
1193

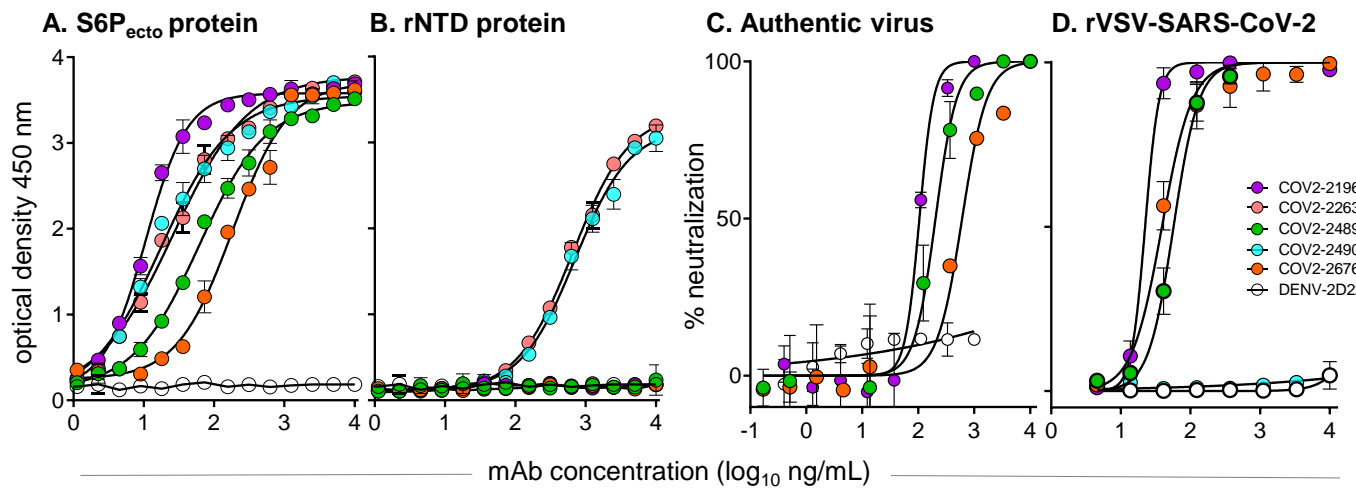
- 1194 Wu, N.C., Yuan, M., Liu, H., Lee, C.D., Zhu, X., Bangaru, S., Torres, J.L., Caniels, T.G.,
1195 Brouwer, P.J.M., van Gils, M.J., et al. (2020). An alternative binding mode of IGHV3-53
1196 antibodies to the SARS-CoV-2 receptor binding domain. *Cell Rep* 33, 108274.
1197
- 1198 Yu, J., Tostanoski, L.H., Peter, L., Mercado, N.B., McMahan, K., Mahrokhian, S.H., Nkolola,
1199 J.P., Liu, J., Li, Z., Chandrashekar, A., et al. (2020). DNA vaccine protection against SARS-
1200 CoV-2 in rhesus macaques. *Science* 369, 806-811.
1201
- 1202 Zhang, L., Cao, L., Gao, X.-S., Zheng, B.-Y., Deng, Y.-Q., Li, J.-X., Feng, R., Bian, Q., Guo,
1203 X.-L., Wang, N., et al. (2020). A proof of concept for neutralizing antibody-guided vaccine
1204 design against SARS-CoV-2. *bioRxiv*, 2020.2009.2023.309294.
1205
- 1206 Zhou, H., Chen, Y., Zhang, S., Niu, P., Qin, K., Jia, W., Huang, B., Zhang, S., Lan, J., Zhang, L.,
1207 et al. (2019). Structural definition of a neutralization epitope on the N-terminal domain of
1208 MERS-CoV spike glycoprotein. *Nat Commun* 10, 3068.
1209
- 1210 Zost, S.J., Gilchuk, P., Case, J.B., Binshtein, E., Chen, R.E., Nkolola, J.P., Schafer, A., Reidy,
1211 J.X., Trivette, A., Nargi, R.S., et al. (2020a). Potently neutralizing and protective human
1212 antibodies against SARS-CoV-2. *Nature* 584, 443-449.
1213
- 1214 Zost, S.J., Gilchuk, P., Chen, R.E., Case, J.B., Reidy, J.X., Trivette, A., Nargi, R.S., Sutton, R.E.,
1215 Suryadevara, N., Chen, E.C., et al. (2020b). Rapid isolation and profiling of a diverse panel of
1216 human monoclonal antibodies targeting the SARS-CoV-2 spike protein. *Nat Med* 26, 1422-1427.

1217

Figure 1

ELISA binding

Neutralization



E. Competition-binding ELISA

F. ACE2 blocking ELISA

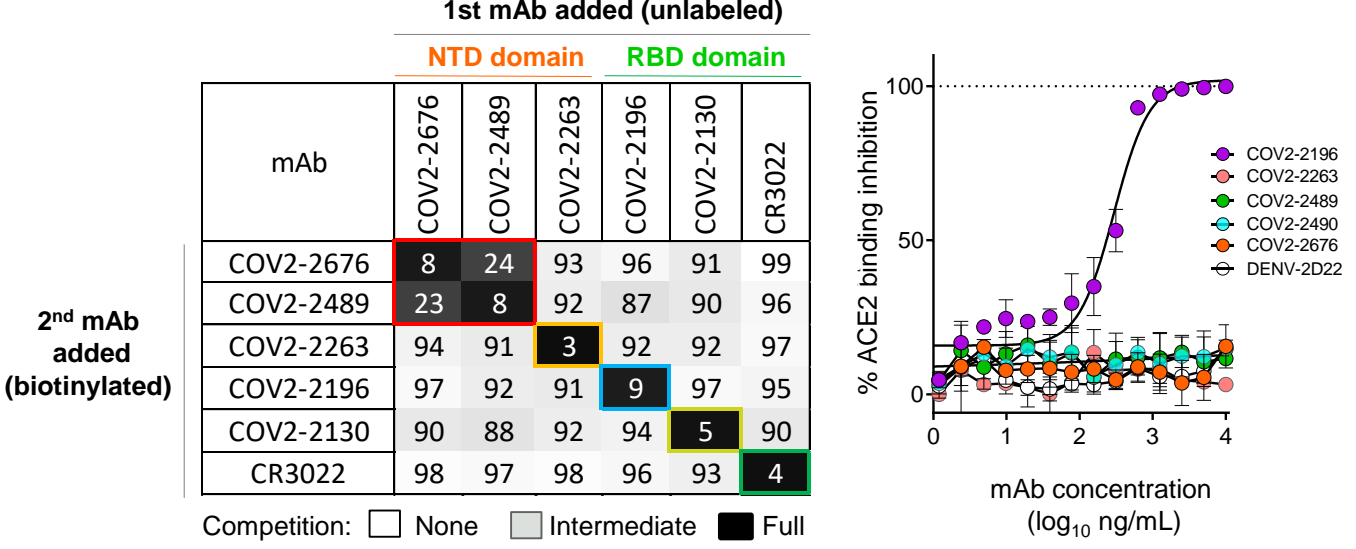
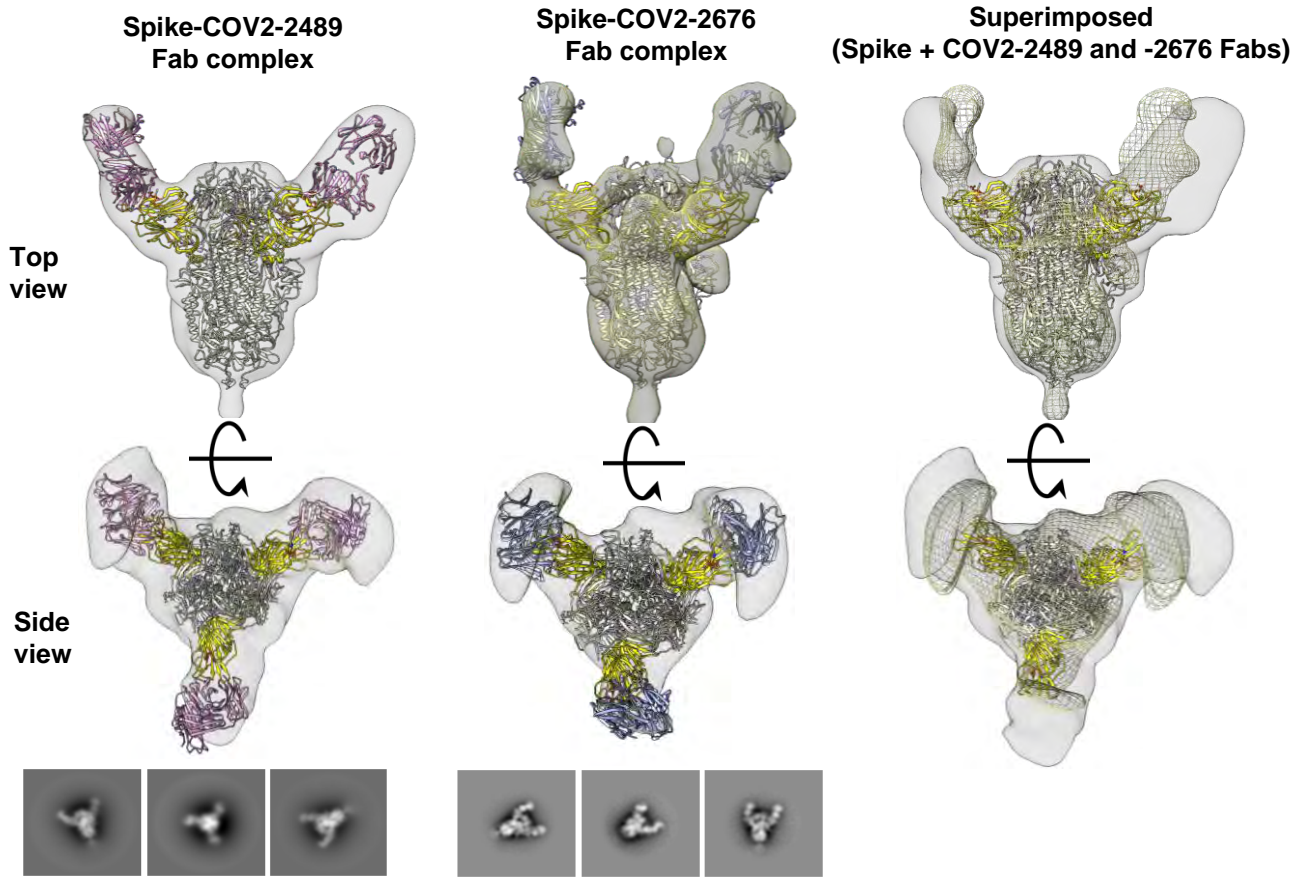
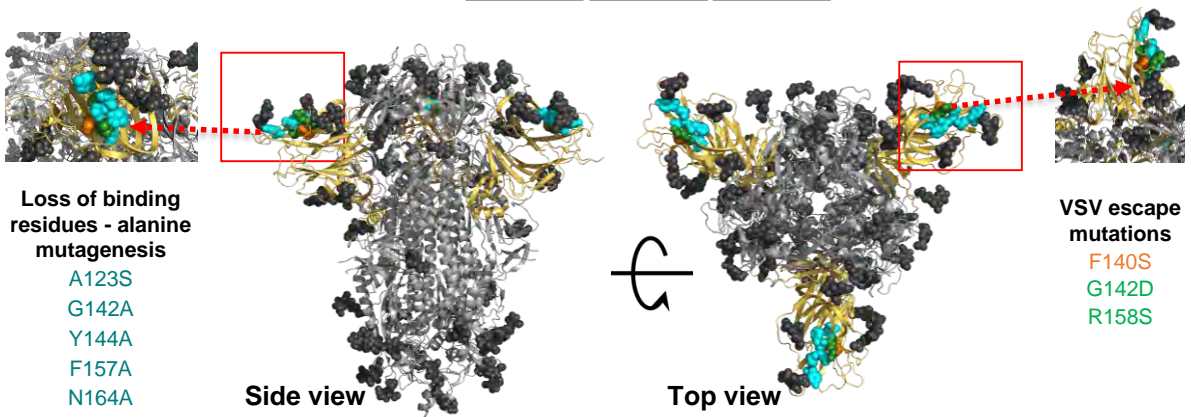


Figure 2

A



B



C

Features of escape mutant virus selection	MAb used for escape selection	
	COV2-2489	COV2-2676
Number of wells escaped of wells tested with mAb	5 of 88 (5.6 %)	1 of 88 (1.1 %)
Mutations selected (number of times)	G142D (twice) R158S (3 times)	F140S (once)

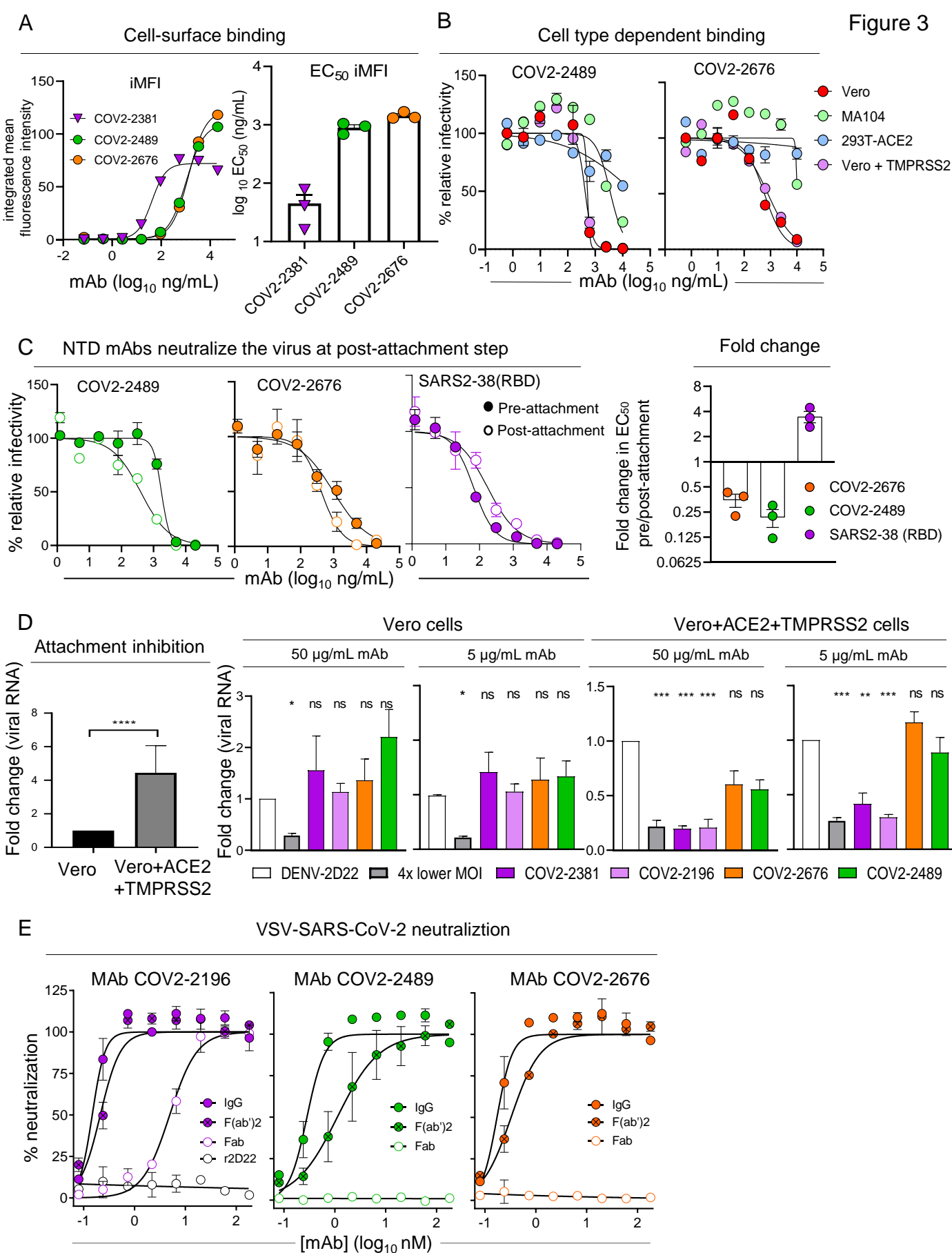
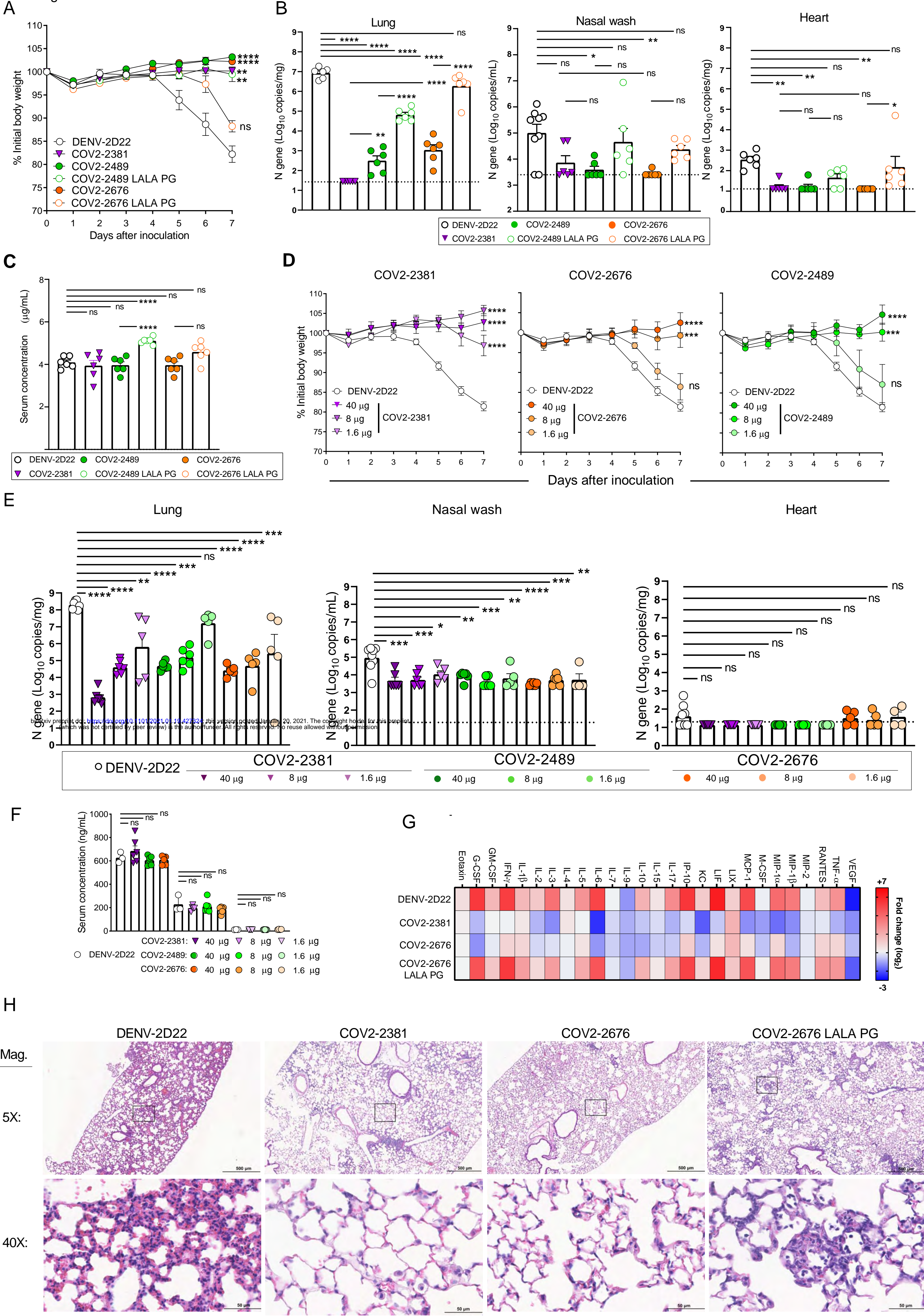
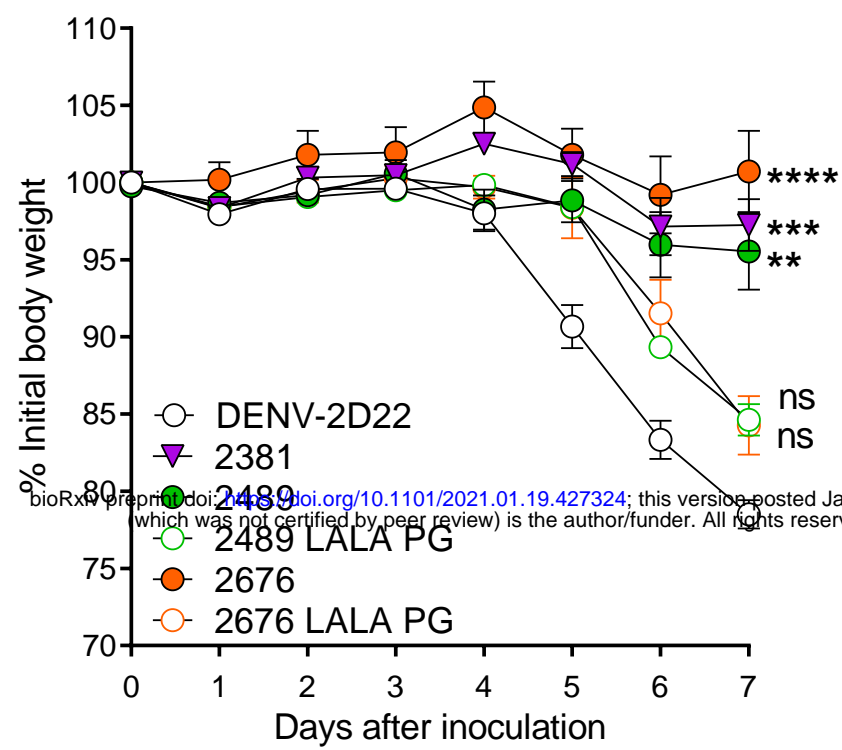


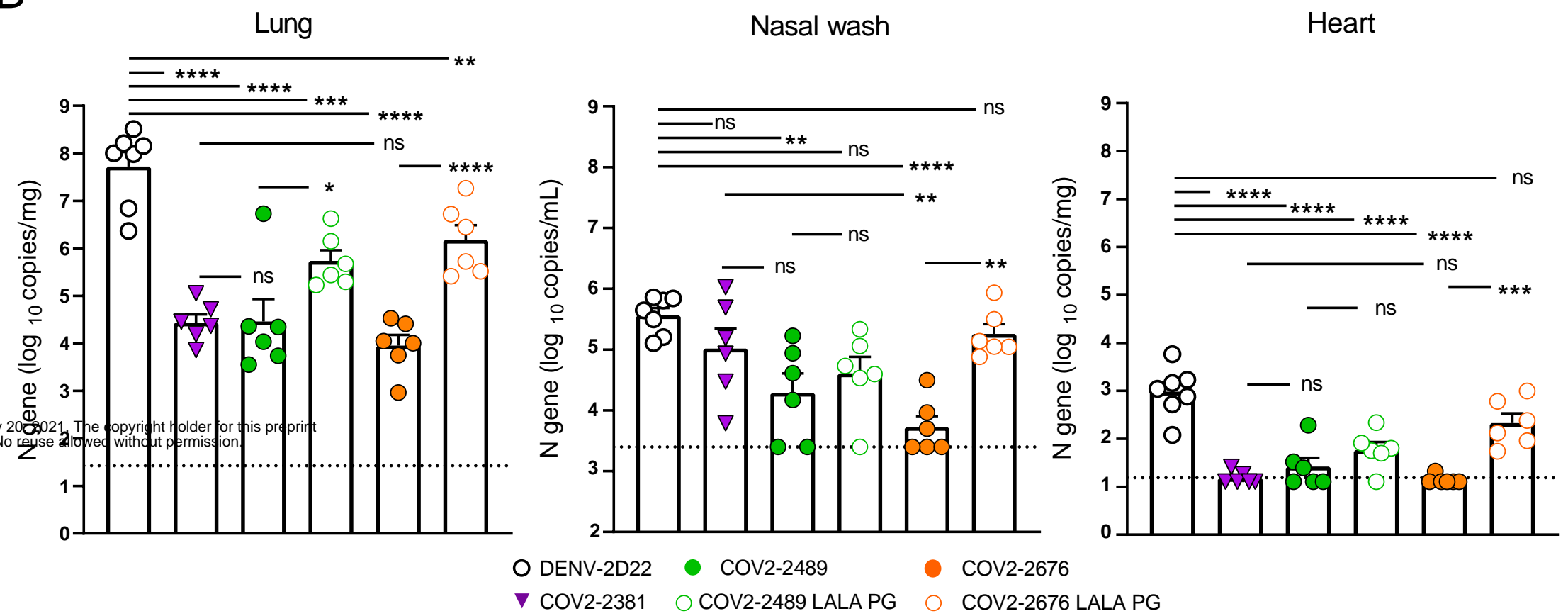
Figure 4



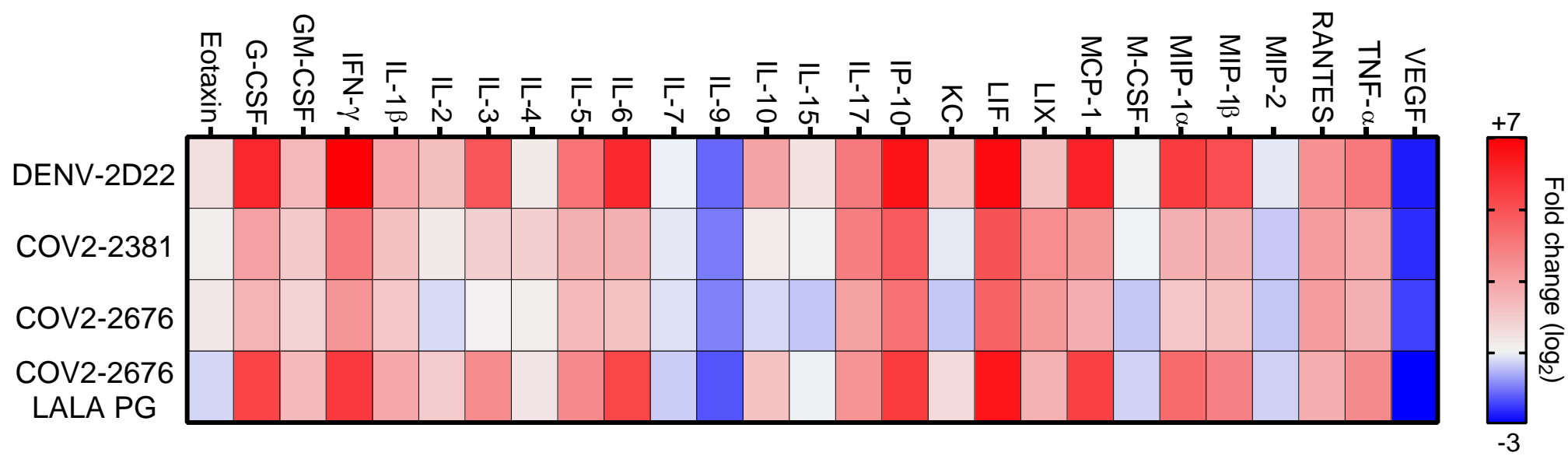
A Figure 5



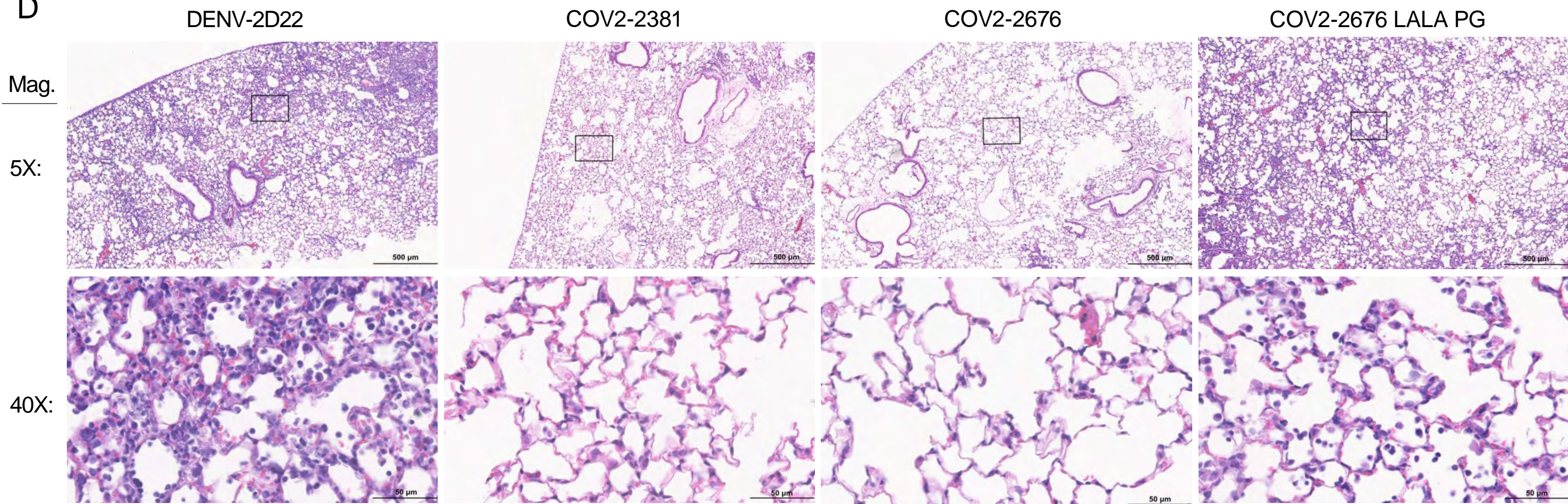
B



C



D

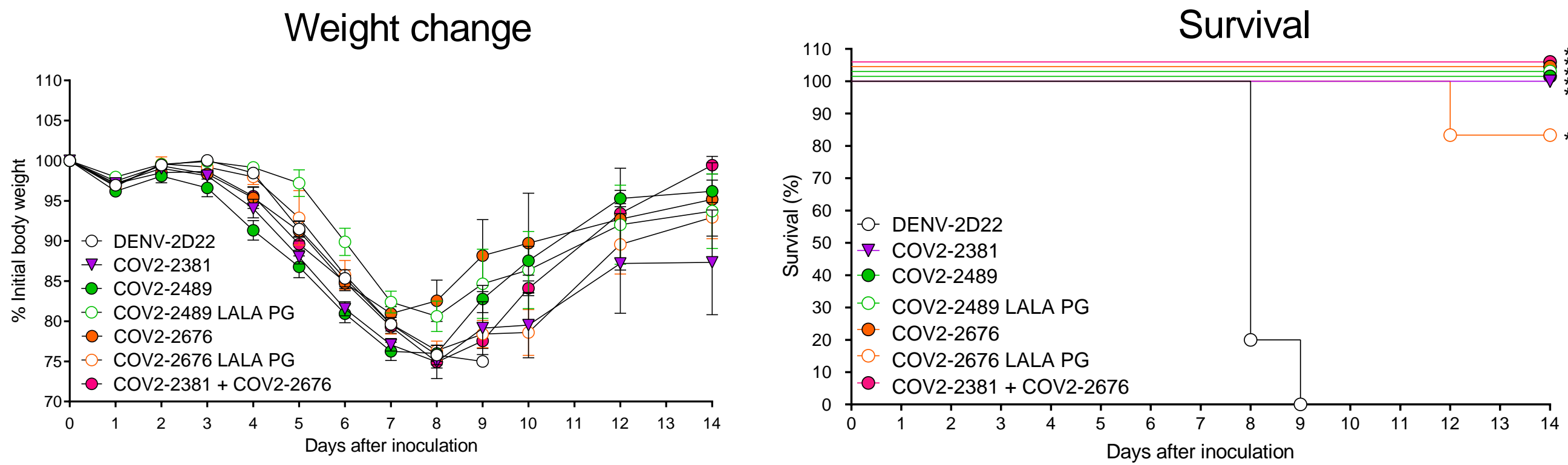


A Figure 6

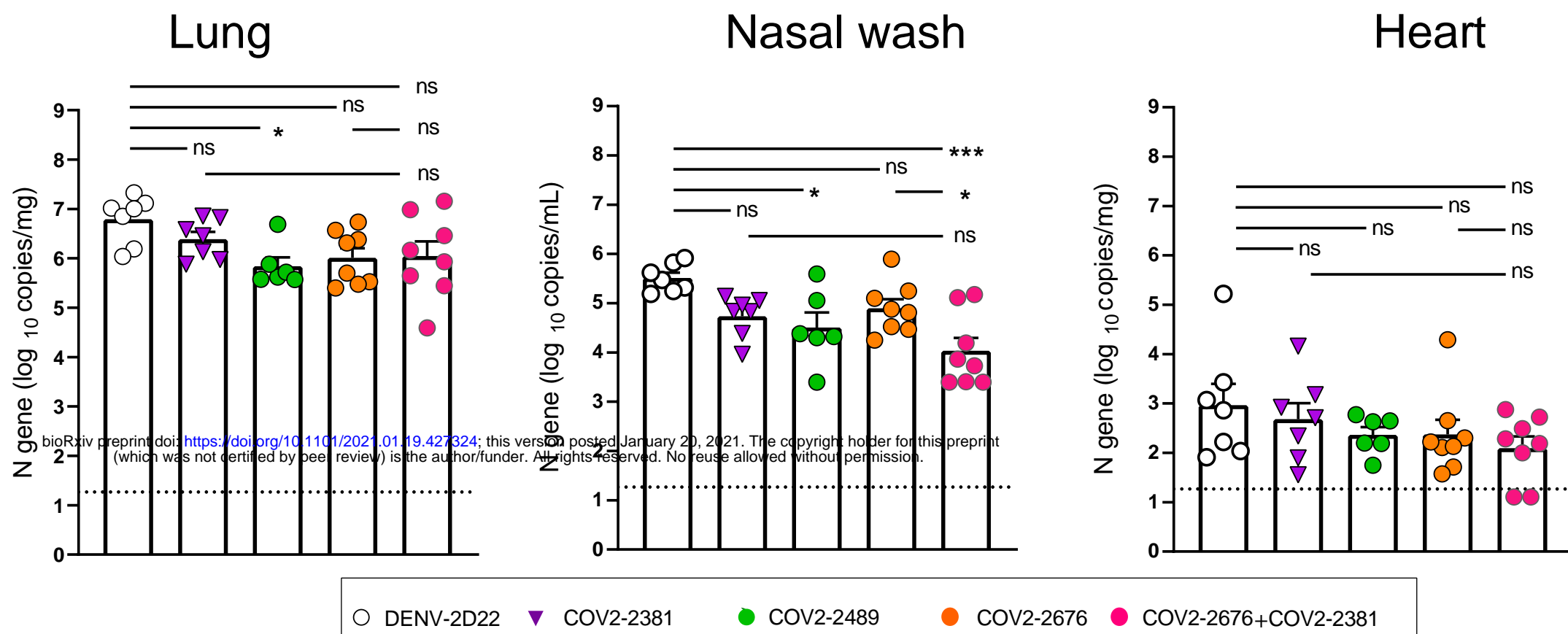
			MAb tested for neutralization of escape virus			
Antigenic site	MAb used to select escape virus	Mutation identified in escape virus	COV2-2479	COV2-2130	COV2-2489	COV2-2676
RBD	COV2-2479 *	E484K	4	97	96	99
	COV2-2130 *	K444R	100	8	101	99
NTD	COV2-2489-1	G142D	92	97	-3	7
	COV2-2489-2	R158S	90	97	-3	-1
	COV2-2676	F140S	93	98	13	18

-5 105
% neutralization

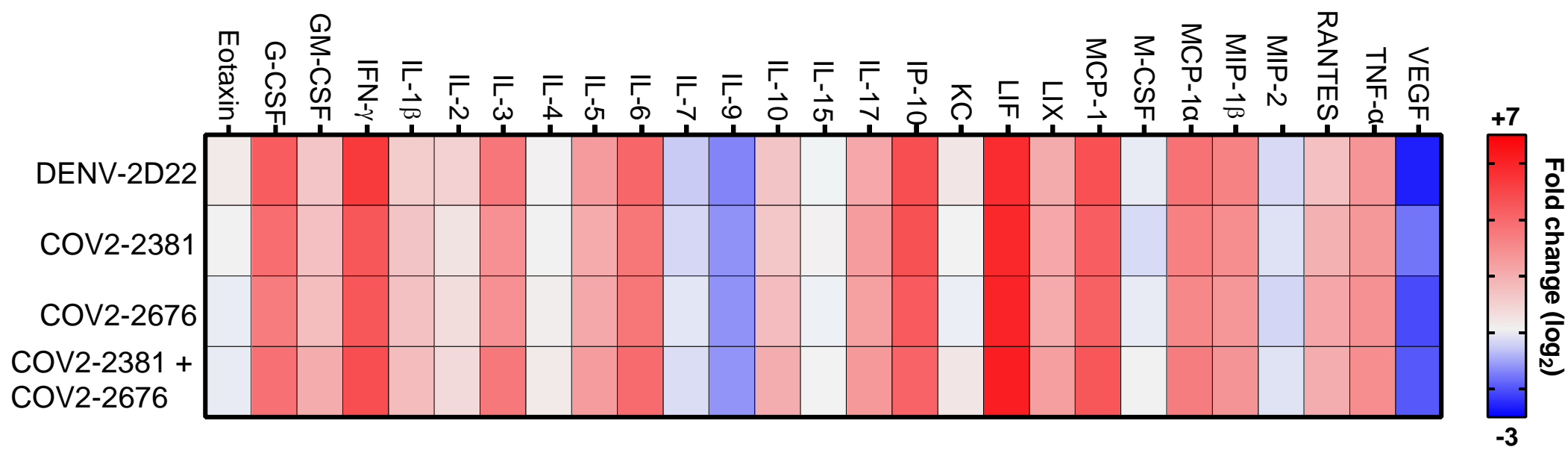
B



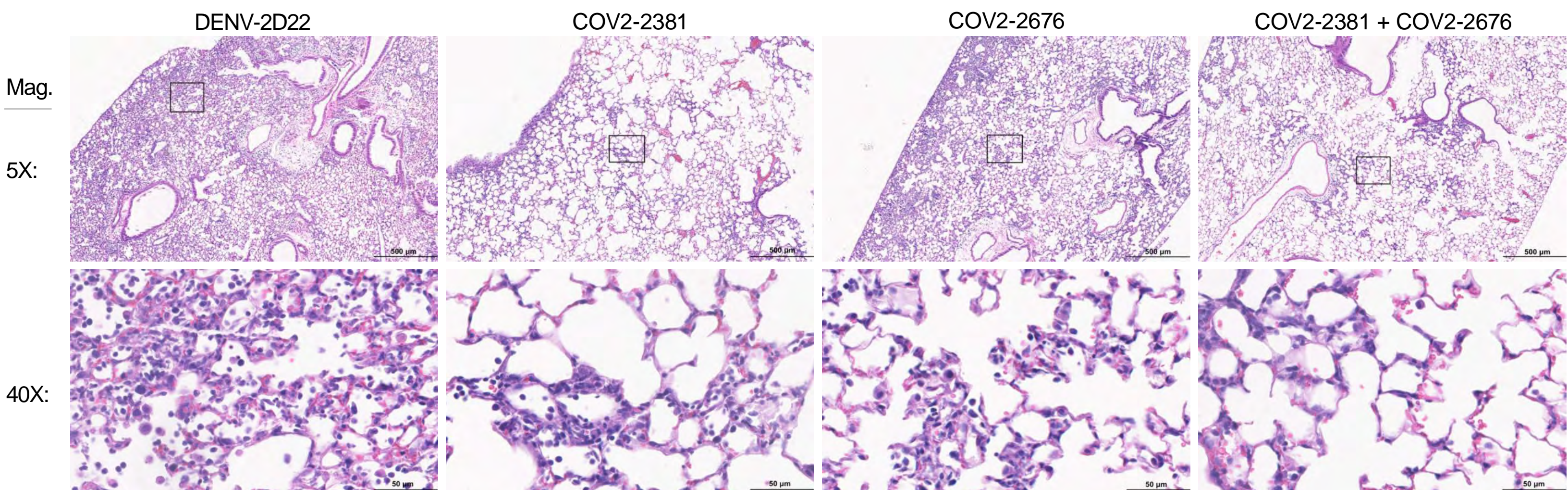
C



D



E



Competition binding

		Second mAb added																																				
1st mAb added:	mAb name	COV2-2016	COV2-2021	COV2-2026	COV2-2130	COV2-2196	COV2-2251	COV2-2257	COV2-2260	COV2-2263	COV2-2293	COV2-2305	COV2-2335	COV2-2346	COV2-2384	COV2-2394	COV2-2405	COV2-2438	COV2-2444	COV2-2455	COV2-2459	COV2-2466	COV2-2489	COV2-2490	COV2-2495	COV2-2525	COV2-2526	COV2-2533	COV2-2558	COV2-2563	COV2-2571	COV2-2622	COV2-2673	COV2-2676	COV2-2769	COV2-2816	COV2-2830	CR3022
	COV2-2263		97	88	91	92	92	80	94	91	13	90	82	82	93	84	88	98	90	91	84	79	86	91	93	92	89	89	98	91	86	53	75	88	96	92	95	95
COV2-2676		45	60	79	91	96	95	85	92	93	95	96	89	92	91	94	95	89	89	93	91	87	23	72	73	86	67	90	87	92	96	97	94	10	66	96	90	99

Figure S1. Competition binding of NTD-reactive MAbs

Competition of the panel of neutralizing mAbs with reference mAbs COV2-2676 and COV2-2263. Binding of reference mAbs to trimeric S-6P_{ecto} was measured in the presence of a saturating concentration of competitor mAb in a competition ELISA and normalized to binding in the presence of rDENV-2D22. Black indicates full competition (<25% binding of reference antibody); grey indicates partial competition (25 to 60% binding of reference antibody); white indicates no competition (>60% binding of reference antibody).

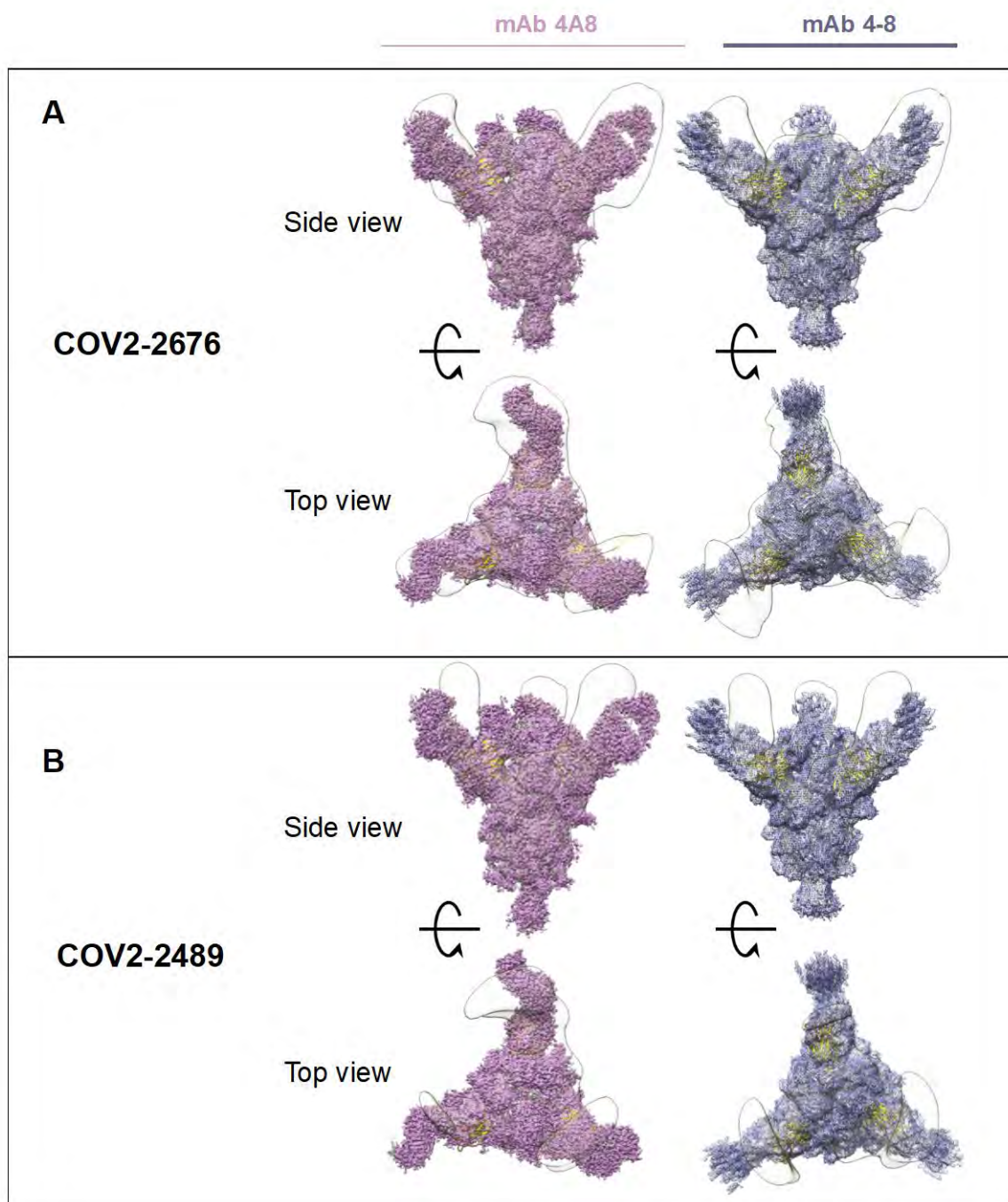
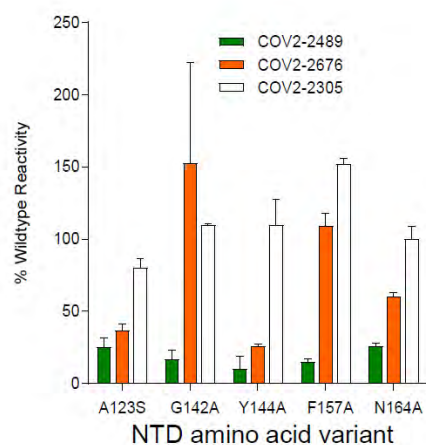


Figure S2. Superimposed Fab-Spike negative stain EM

A) COV2-2676 with mAb on the top is side view 4A8 (left), mAb 4-8 (right) and bottom is top view of the same.

B) COV2-2489 with mAb on the top is side view 4A8 (left), mAb 4-8 (right) and bottom is top view of the same.

A



B

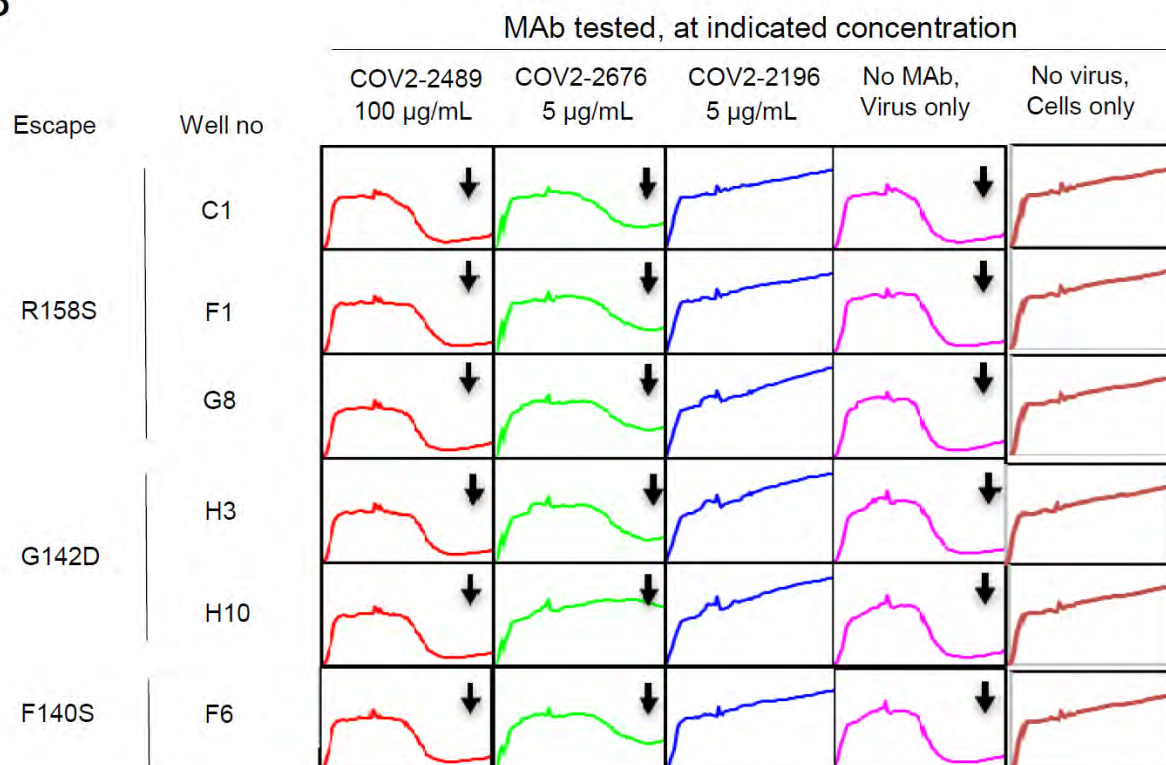
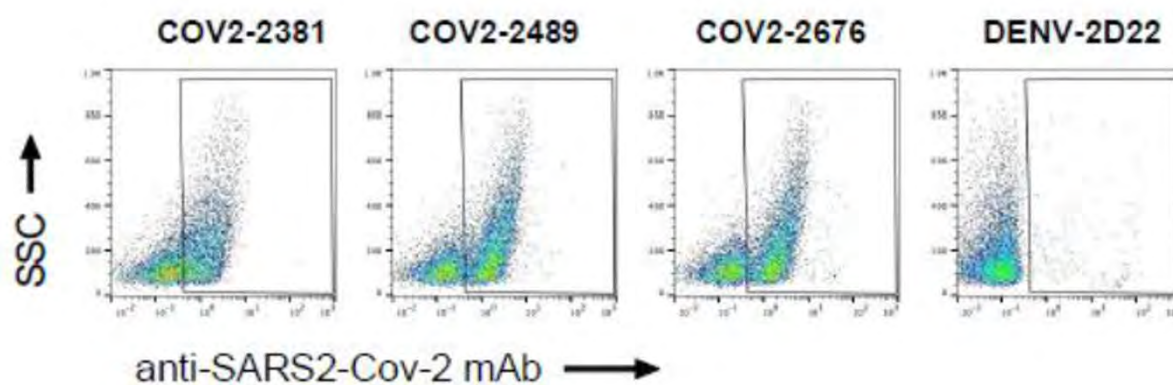
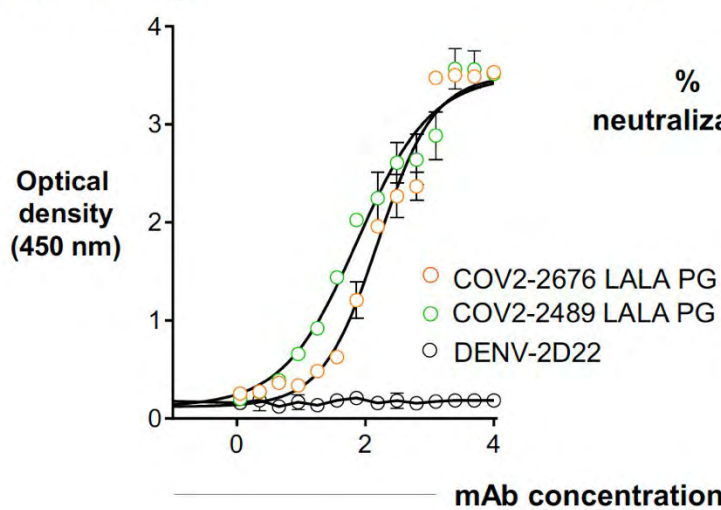


Figure S3. A) Identification of critical contact residues by alanine mutagenesis. Binding values for mAbs COV2-2489, -2676, and -2305. The binding values are shown as a percentage of mAb binding to wild-type (WT) SARS-CoV-2 spike protein and are plotted with the range (highest-minus lowest binding value) of at least two measurements. **B) Real-time cell analysis (RTCA) to select for spike-protein-expressing VSV viruses that escape antibody neutralization, related to Figure 2 B & C.** Example sensograms from individual wells of 96-well E-plate analysis showing viruses that escaped neutralization (noted with arrow) by indicated antibodies. Cytopathic effect (CPE) was monitored kinetically in Vero E6 cells inoculated with virus in the presence of a saturating concentration of antibody COV2-2489 at 100 µg/mL (red), COV2-2676 at 5 µg/mL (green) or lack of escape using RBD-specific mAb COV2-2196-blue at 5 µg/mL (blue) are shown. Uninfected cells (brown) or cells inoculated with virus without antibody (magenta) serve as controls. All curves represented show a mean of technical duplicates.

A. Gating strategy



B. Binding



C. Neutralization

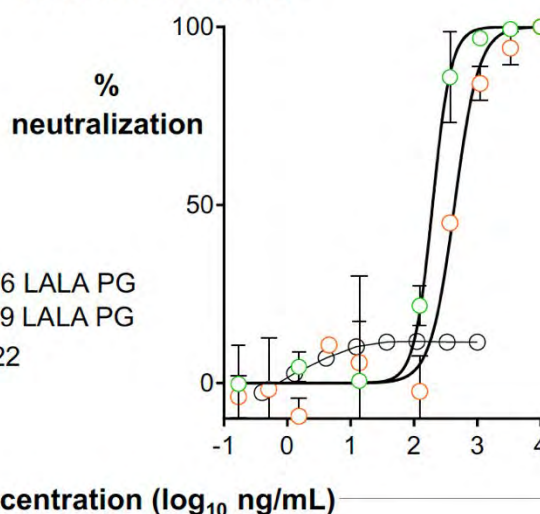


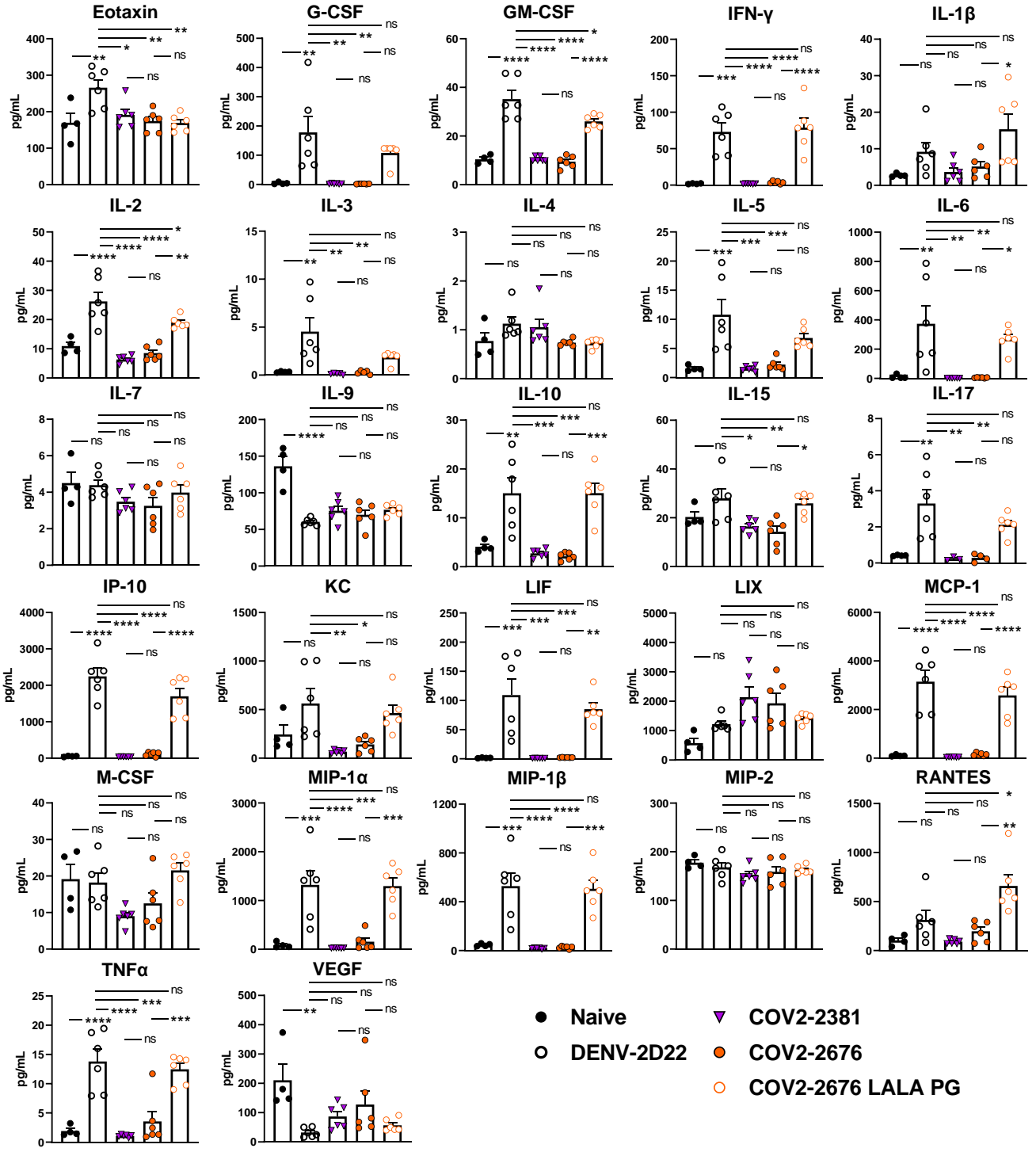
Figure S4. Gating strategy of Vero-E6 cells infected with SARS-CoV-2 for cell surface-displayed spike protein binding assay and ELISA and FRNT for COV2-2676 and COV2-2489 mAbs made with LALA-PG Fc variants.

A. A representative gating strategy illustrating stained with primary COV2-2381, COV2-2676, COV2-2489 or DENV-2D22 MAb.

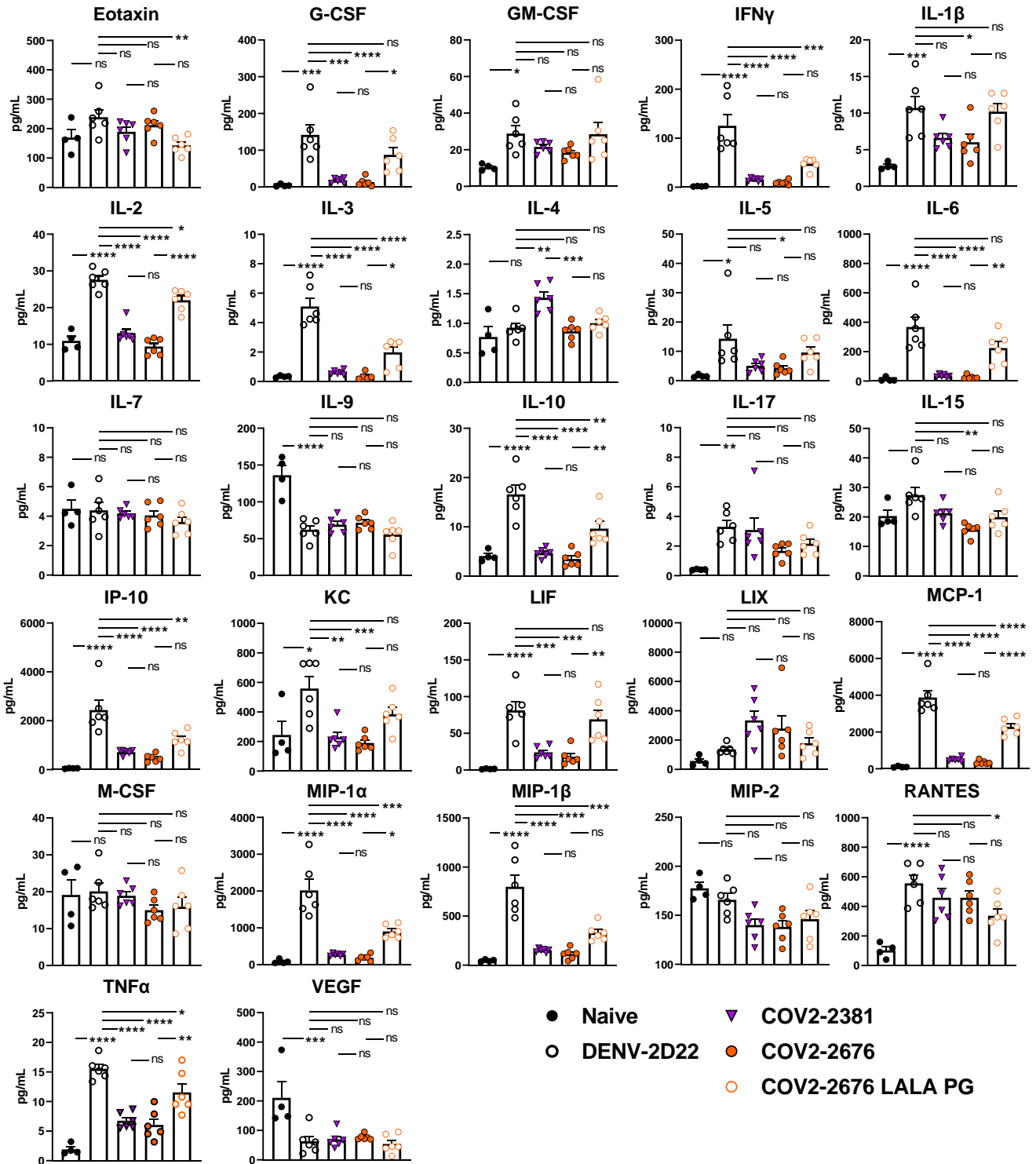
B. ELISA binding of COV2-2676-LALA-PG, COV2-2489-LALA-PG or DENV-2D22 to trimeric S-6P_{ecto}. Data are mean \pm S.D. of technical triplicates from a representative experiment repeated twice.

C. Neutralization curves for COV2-2676-LALA-PG, 2489-LALA-PG or DENV-2D22 using wild-type authentic SARS-CoV-2 in a FRNT assay. Error bars indicate S.D.; data represent at least two independent experiments performed in technical duplicate.

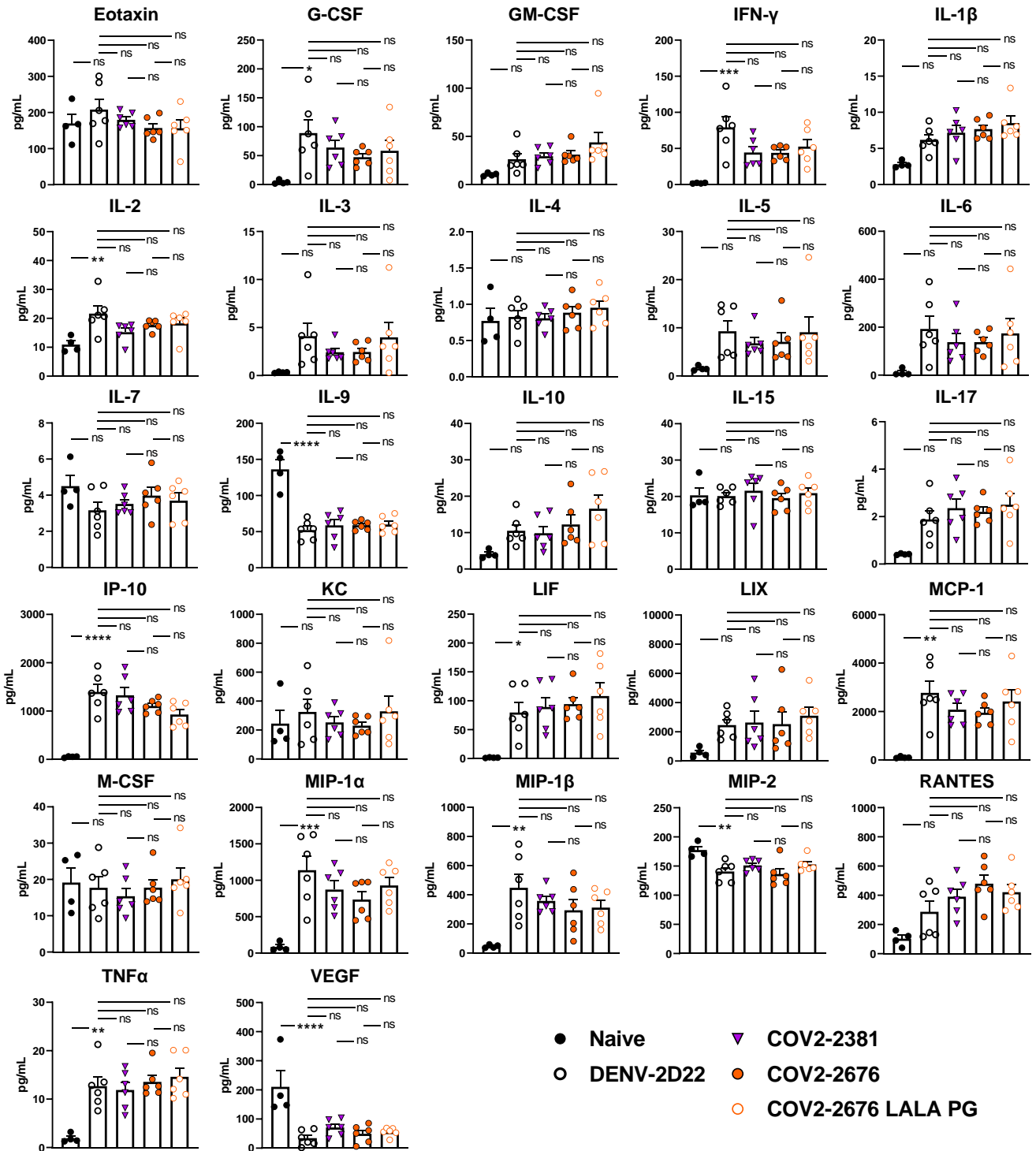
D-1



D+1



D+2



● Naive ▼ COV2-2381
 ○ DENV-2D2 ● COV2-2676
 ○ COV2-2676 LALA PG

Figure. S5A-C. Cytokine and chemokine levels in the lungs of SARS-CoV-2 infected mice .

- A. Cytokine and chemokine levels in the lungs of SARS-CoV-2 infected mice at 7 dpi following d-1 treatment with isotype, COV2-2381, COV2-2676, and COV2-2676 LALA PG as measured by a multiplex platform (two independent experiments, n = 6 per group. One-way ANOVA with Tukey's post hoc test: ns, not significant, *p < 0.05, **p < 0.01, ***p < 0.001, ****p < 0.0001.)
- B. Cytokine and chemokine levels in the lungs of SARS-CoV-2 infected mice at 7 dpi following d+1 treatment with isotype, COV2-2381, COV2-2676, and COV2-2676 LALA PG as measured by a multiplex platform (two independent experiments, n = 6 per group. One-way ANOVA with Tukey's post hoc test: ns, not significant, *p < 0.05, **p < 0.01, ***p < 0.001, ****p < 0.0001.)
- C. Cytokine and chemokine levels in the lungs of SARS-CoV-2 infected mice at 7 dpi following d+1 treatment with isotype, COV2-2381, COV2-2676, and COV2-2676 LALA PG as measured by a multiplex platform (two independent experiments, n = 6 per group. One-way ANOVA with Tukey's post hoc test: ns, not significant, *p < 0.05, **p < 0.01, ***p < 0.001, ****p < 0.0001.)